GRASSMANNIAN SPECTRAL SHOOTING

VEERLE LEDOUX[1], SIMON J.A. MALHAM[2] AND VERA THÜMMLER[3]

Abstract. We present a new numerical method for computing the pure-point spectrum associated with the linear stability of coherent structures. In the context of the Evans function shooting and matching approach, all the relevant information is carried by the flow projected onto the underlying Grassmann manifold. We show how to numerically construct this projected flow in a stable and robust manner. In particular, the method avoids representation singularities by, in practice, choosing the best coordinate patch representation for the flow as it evolves. The method is analytic in the spectral parameter and of complexity bounded by the order of the spectral problem cubed. For large systems it represents a competitive method to those recently developed that are based on continuous orthogonalization. We demonstrate this by comparing the two methods in three applications: Boussinesq solitary waves, autocatalytic travelling waves and Ekman boundary layer.

1. Introduction

We introduce a new numerical method for solving high order linear spectral problems by shooting and matching. The numerical construction of pure-point spectra is important in determining the linear stability of coherent structures. Examples of such structures are: ground and higher excited states of molecules in quantum chemistry (Johnson [56], Hutson [51], Gray and Manopoulous [39], Manopoulous and Gray [69], Chou and Wyatt [23, 24], Ledoux [64], Ledoux, Vand Daele and Vanden Berghe [65], Ixaru [55]); nonlinear travelling fronts in reaction-diffusion such as autocatalysis or combustion (Billingham and Needham [9], Metcalf, Merkin and Scott [72], Doelman, Gardner and Kaper [31], Terman [95], Gubernov, Mercer, Sidhu and Weber [41]); nerve impulses (Alexander, Gardner and Jones [2]), neural waves (Coombes and Owen [25]); solitary waves or steady flows over compliant surfaces (Pego and Weinstein [82], Alexander and Sachs [3], Chang, Demekhin and Kopelevich [21], Kapitula and Sandstede [57], Bridges, Derks and Gottwald [14], Allen [4], Allen and Bridges [5]); laser pulses (Swinton and Elgin [94]); nonlinear waves along elastic rods (Lafortune and Lega [62]); ionization fronts (Derks, Ebert and Meulenbroek [28]) or spiral waves (Sandstede and Scheel [89]).

For such problems the matching condition is typically a discriminant known as the Evans function (Evans [34], Alexander, Gardner and Jones [2]) or miss-distance function (Pryce [85], Greenberg and Marletta [39]). It measures the degree of (possibly transversal) intersection of the stable and unstable solution subspaces satisfying the longitudinally separated far field boundary data. The stable subspace decays in the direction of wave propagation whilst the unstable subspace decays in the

Date: 2nd September 2008.
2000 *Mathematics Subject Classification.* 65L15, 65L10.
Key words and phrases. Grassmann manifolds, spectral theory, numerical shooting.

opposite direction. Equivalently, the Evans function is the determinant of the set of solution vectors spanning both subspaces. With this end-goal matching condition in mind, the problem boils down to how to numerically construct the solution subspaces in a robust fashion, as well as where to match longitudinally. This is especially difficult for large scale problems. These might either emerge from high order systems, or more specifically, we envisage the stability of nonlinear travelling waves with multi-dimensional structure; for example wrinkled fronts travelling in a fixed longitudinal direction. The transverse structural information can be projected onto finite dimensional transverse basis, generating a large linear spectral problem posed on the one-dimensional longitudinal coefficient function set (see Ledoux, Malham, Niesen and Thümmler [66]). Hitherto such large problems could not be solved by shooting and matching and were resolved by projecting the whole problem onto a finite basis and solving the resulting large algebraic eigenvalue problem. However recently, in the context of the Evans function, Humpherys and Zumbrun [49] proposed continuous orthogonalization as a viable approach to help make large scale problems amenable to shooting and matching. Here we provide our own answer.

We propose the *new* Grassmann Gaussian elimination method (GGEM) which resolves several numerical problems all in one, in particular it:

(1) Evolves the solution along the underlying Grassmann manifold avoiding representation singularities.
(2) Retains analyticity in the spectral parameter.
(3) Allows for matching anywhere in the longitudinal computational domain.
(4) Has polynomial complexity, operations are of the order of the size of the system cubed.
(5) Naturally evolves the solution in what in practice is the optimal coordinate representation (generated by optimal partial pivoting).

For each property what is new, expected, proved, numerically observed, and its context?

First, evolving the solution subspaces, considered as curves in the Grassmann manifold is not new for autonomous problems—see Hermann and Martin [44, 45, 46, 47, 48], Martin and Hermann [71] Brockett and Byrnes [18], Shayman [91], Rosenthal [87], Ravi, Rosenthal and Wang [86], Zelikin [99], Abou–Kandil, Freiling, Ionescu and Jank [1] and Bittanti, Laub and Willems [12]. Using Riccati systems to solve nonautonomous spectral problems is also not new—see Johnson [56], Hutson [51], Pryce [85], Manopoulous and Gray [69], Gray and Manopoulous [38] and Chou and Wyatt [23, 24]. Here Riccati systems correspond to the flow of the linear spectral problem projected onto the Grassmann manifold with a fixed coordinate patch representation. See Schiff and Shnider [90] and Chou and Wyatt [24] who use this connection to integrate Riccati systems through singularities.

That we have a numerical method that avoids representation singularities for nonautonomous systems is *new*. The idea is as follows. Given data that lies in a suitable coordinate patch of the Grassmann manifold, pullback to the Stiefel manifold. Evolve the solution one steplength along the Stiefel manifold either directly using a Runge–Kutta method or a Lie group method. Then project onto a suitable and possibly different coordinate patch of the Grassmann manifold using optimal Gaussian elimination. In this last step, the practical method we propose picks a quasi-optimal coordinate patch in which to best represent the solution in the Grassmann manifold (see below and Section 5).

Note that on first inspection the Stiefel manifold is the direct natural setting for the stable and unstable solution subspaces. Afterall in each case we have to construct the full set of solutions to a large system of differential equations satisfying the correct respective asymptotic boundary conditions in the far field. Each solution set represents a curve in the Stiefel manifold of dimension commensurate with the size of the solution set. That the spectral problems are linear means that all the relevant spectral information can be reconstructed from the flow in the corresponding Grassmann manifold. That the matching condition is determinental, means that we only need the Grassmann flow information—see Martin and Hermann [71] and Brockett and Byrnes [18] where this reduction was first considered for autonomous linear control problems (in practice we will also need to retain a complex scalar field to ensure analytic dependence on parameters). This reduction is crucial because long-range integration along the Stiefel manifold has been problematic (due to multiple distinct exponential growth and decay rates) and one of the simplest resolutions in the Evans function context was to use Plücker coordinates—whilst ignoring the Plücker relations (more on these below).

Second, retaining analyticity away from the essential spectrum is *standard* for any shooting method; we prove analyticity in Section 5. This allows for a global search for eigenvalues in that region by numerically computing the change in argument of the Evans function round any closed contour. Invoking the argument principle, this integer value represents the number of zeros of the Evans function, and hence the number of eigenvalues counting multiplicity, inside the contour; see Brockett and Byrnes [18], Alexander, Gardner and Jones [2] and Ying and Katz [98].

Third, that our method allows matching anywhere in the longitudinal domain is *new*. We provide substantive numerical evidence. Previously, other than in trivial cases, most numerical practioners used the common-sense rule of thumb of integrating the spectral problem from both ends of the longitudinal domain and matching at a point roughly centered on the front (which is assumed to be localized). When solving the linear problem with Plücker coordinates, it was first important to rescale for the far field spatial behaviour to neutralize its total exponential growth. Integrating from the far field initial conditions (a subset of the spatial eigenvectors), the solution remains roughly constant until the coefficient matrix starts to reveal its nonautonmous character due to the integration step impinging on the front. Accuracy is retained whilst integrating through the front, but thereafter the problem becomes stiff. The issue is that the numerical methods cannot resolve the simultaneous exponential growth and decay character associated with the other far-end stable and unstable subspaces.

Fourth, having polynomial complexity is *essential* and we provide here a *new* alternate. After Humpherys and Zumbrun [49] introduced their continuous orthogonalization method in this context, which also has polynomial complexity, any new numerical spectral shooting method should have this property and also be competitive. Previous successful methods used Plücker coordinates, ignoring the quadratic Plücker relations (see Section 2). They solved the flow for the corresponding linear vector field in the higher dimensional Plücker embedding space. Details of this Plücker coordinate or compound matrix approach can be found in, for example, Alexander and Sachs [3], Brin [16, 17] and Allen and Bridges [5]. Unfortunately the number of Plücker coordinates typically grows exponentially with the order of

the original system, and so this approach cannot be used for medium to large order systems. However the continuous orthogonalization method of Humpherys and Zumbrun, and our method, are especially suited to large scale problems.

Fifth, our method for dynamic *practical optimal* coordinate representation is *new*. Given data on the Stiefel manifold, for example generated by advancing the solution one steplength along the Stiefel manifold, how can we project down onto the Grassmann manifold using the best representation patch possible? The idea is as follows. The natural map projection from the Stiefel to the Grassmann manifolds is a linear fractional map (Milnor and Stasheff [74]; Martin and Hermann [71]). This map represents the action of equivalencing by transformations whose rank matches that of the Stiefel manifold (this takes us from the space of frames to the space of spaces spanning those frames). The Stiefel manifold has a non-square matrix representation. Projection onto the Grassmann manifold corresponds to equivalencing by a full rank minor of the non-square Stiefel matrix—this renders the corresponding minor as the identity matrix. We are free to choose which minor to equivalence by, each distinct choice corresponds to the matrix representation of a coordinate patch on the Grassmann manifold. We can use Gaussian elimination, via elementary column operations, to render any given full rank minor of the Stiefel matrix as the identity matrix. The key is to try to pick the minor which has the largest determinant—this corresponds to choosing the Grassmannian patch that gives the best representation for the projection from the Stiefel to Grassmann manifold. Ideally we would check the size of every minor of the Stiefel matrix and equivalence by the one with the largest determinant. However this is an NP problem (equivalent to using the Plücker coordinates described above). We provide a practical solution of polynomial complexity. The method maximises the pivot used at each step of the Gaussian elimination process. In the current context, we call it quasi-optimal Gaussian elimination.

Our paper is organised as follows. In Section 2, we provide a tailored review of Grassmann manifolds and their representation. We then show, in Section 3 how flows generated by linear vector fields on the Stiefel manifold, produce a natural flow on the underlying Grassmann manifold that is decoupled from the flow through the remaining fibres. We subsequently show how this leads to using Riccati systems to resolve spectra, but that singularities that develop in the Riccati flows present spectral matching problems. In Section 4 we introduce two new practical approaches to avoiding these representation singularities. One is the idea behind our main method, the Grassmann Gaussian elimination method. The other is a modification of the Riccati approach that changes the coordinate patch when deemed necessary. Also in this section we show the connection between the Riccati and continuous orthogonalization approaches. We present our proposed Grassmann Gaussian elimination method fully in Section 5, including details of how in practice to choose the quasi-optimal Grassmannian coordinate representation patch. We review the Evans function in Section 6 and discuss a some further simple practical numerical refinements that prevent potential numerical overflow. We then implement and compare all the competing numerical methods in Section 7 in three distinct applications. Finally in Section 8 we conclude and present future directions of research.

2. Review: Grassmann manifolds

2.1. **Grassmann and Stiefel manifolds.** A k-frame is a k-tuple of $k \leq n$ linearly independent vectors in $\mathbb{C}^n$. The *Stiefel manifold* $\mathbb{V}(n,k)$ of k-frames is the open subset of $\mathbb{C}^{n\times k}$ of all k-frames centred at the origin. The set of k dimensional subspaces of $\mathbb{C}^n$ form a complex manifold $\mathrm{Gr}(n,k)$ called the *Grassmann manifold* of k-planes in $\mathbb{C}^n$ (see Steenrod [88, p. 35] or Griffiths and Harris [40, p. 193]).

The fibre bundle $\pi\colon \mathbb{V}(n,k)\to\mathrm{Gr}(n,k)$ is a *principle fibre bundle*. For each y in the base space $\mathrm{Gr}(n,k)$, the inverse image $\pi^{-1}(y)$ is homeomorphic to the fibre space $\mathrm{GL}(k)$ which is a Lie group—see Montgomery [76, p. 151]. In fact, it is a trivial fibre bundle as $\mathbb{V}(n,k) \cong \mathrm{Gr}(n,k)\times\mathrm{GL}(k)$. The projection map π is the natural quotient map sending each k-frame centered at the origin to the k-plane it spans—see Milnor and Stasheff [74, p. 56].

2.2. **Representation.** Following the exposition in Griffiths and Harris [40], any k-plane in $\mathbb{C}^n$ can be represented by an $n\times k$ matrix of rank k, say $Y \in \mathbb{C}^{n\times k}$. Any two such matrices Y and Y' represent the same k-plane element of $\mathrm{Gr}(n,k)$ if and only if $Y' = Yu$ for some $u \in \mathrm{GL}(k)$ (the k-dimensional subspace elements are invariant to rank k closed transformations mapping k-planes to k-planes).

Let $\mathfrak{i} = \{i_1,\dots,i_k\} \subset \{1,\dots,n\}$ denote a multi-index of cardinality k. Let $Y_{\mathfrak{i}^\circ} \subset \mathbb{C}^n$ denote the $(n-k)$-plane in $\mathbb{C}^n$ spanned by the vectors $\{e_j\colon j \notin \mathfrak{i}\}$ and

$$\mathbb{U}_{\mathfrak{i}} = \left\{Y \in \mathrm{Gr}(n,k)\colon Y \cap Y_{\mathfrak{i}^\circ} = \{0\}\right\}.$$

In other words, $\mathbb{U}_{\mathfrak{i}}$ is the set of k-planes $Y \in \mathrm{Gr}(n,k)$ such that the $k\times k$ minor of one, and hence any, matrix representation of Y is nonsingular (representing a coordinate patch labelled by $\mathfrak{i}$).

Any element of $\mathbb{U}_{\mathfrak{i}}$ has a unique matrix representation $y_{\mathfrak{i}^\circ}$ whose $\mathfrak{i}$th $k\times k$ minor is the identity matrix. For example, if $\mathfrak{i} = \{1,\dots,k\}$ then any element of $\mathbb{U}_{\{1,\dots,k\}}$ can be uniquely represented by a matrix of the form

$$y_{\mathfrak{i}^\circ} = \begin{pmatrix} 1 & 0 & \cdots & 0 \\ 0 & 1 & \cdots & 0 \\ \vdots & \vdots & \ddots & \vdots \\ 0 & 0 & \cdots & 1 \\ \hat{y}_{k+1,1} & \hat{y}_{k+1,2} & \cdots & \hat{y}_{k+1,k} \\ \hat{y}_{k+2,1} & \hat{y}_{k+2,2} & \cdots & \hat{y}_{k+2,k} \\ \vdots & \vdots & \ddots & \vdots \\ \hat{y}_{n,1} & \hat{y}_{n,2} & \cdots & \hat{y}_{n,k} \end{pmatrix},$$

where $\hat{y}_{i,j} \in \mathbb{C}$ for $i = k+1,\dots,n$ and $j = 1,\dots,k$. Conversely, a $n\times k$ matrix of this form represents a k-plane in $\mathbb{U}_{\mathfrak{i}}$. Each coordinate patch $\mathbb{U}_{\mathfrak{i}}$ is an open, dense subset of $\mathrm{Gr}(n,k)$ and the union of all such patches covers $\mathrm{Gr}(n,k)$. For each $\mathfrak{i}$, there is a bijective map $\varphi_{\mathfrak{i}}\colon \mathbb{U}_{\mathfrak{i}} \to \mathbb{C}^{(n-k)k}$ given by

$$\varphi_{\mathfrak{i}}\colon y_{\mathfrak{i}^\circ} \mapsto \hat{y}\,.$$

Each $\varphi_{\mathfrak{i}}$ is thus a local coordinate chart for the coordinate patch $\mathbb{U}_{\mathfrak{i}}$ of $\mathrm{Gr}(n,k)$. For all $\mathfrak{i},\mathfrak{i}'$, if $Y \in \mathbb{U}_{\mathfrak{i}} \cap \mathbb{U}_{\mathfrak{i}'}$ and $u_{\mathfrak{i},\mathfrak{i}'}$ is the $\mathfrak{i}'$th $k\times k$ minor of $y_{\mathfrak{i}^\circ}$, then $y_{(\mathfrak{i}')^\circ} = y_{\mathfrak{i}^\circ}\left(u_{\mathfrak{i},\mathfrak{i}'}\right)^{-1}$. Since $u_{\mathfrak{i},\mathfrak{i}'}$ represents the transformation between representative patchs and depends holomorphically on $y_{\mathfrak{i}^\circ}$, we deduce $\varphi_{\mathfrak{i}} \circ \varphi_{\mathfrak{i}'}^{-1}$ is holomorphic. Note that $\mathrm{Gr}(n,k)$ has a structure of a complex manifold (see Griffiths and Harris [40,

p. 194]). Further the unitary group $\mathbb{U}(n)$ acts continuously and surjectively on $\mathrm{Gr}(n,k)$. Hence $\mathrm{Gr}(n,k)$ is compact and connected. Lastly, the general linear group $\mathrm{GL}(n)$ acts transitively on $\mathrm{Gr}(n,k)$ and it is a homogeneous manifold as it is isomorphic to $\mathrm{GL}(n)/\mathrm{GL}(n-k)\times\mathrm{GL}(k)$ (see Chern [22, p. 65] or Warner [96, p. 130]).

2.3. **Plücker embedding.** There is a natural map, the *Plücker map*,

$$p\colon \mathrm{Gr}(n,k)\to\mathbb{P}\big(\textstyle\bigwedge^k\mathbb{C}^n\big)$$

that sends each k-plane with basis $Y=[Y_1\dots Y_k]$ to $Y_1\wedge\ldots\wedge Y_k$; here $\mathbb{P}^n$ denotes the complex projective space of dimension n. See Griffiths and Harris [40] or Coskun [26] for more details. If we change the basis, the basis for the image changes by the determinant of the transformation matrix. Hence the map is a point in $\mathbb{P}\big(\bigwedge^k\mathbb{C}^n\big)$. We can recover Y from its image $Y_1\wedge\ldots\wedge Y_k$ as the set of all vectors v such that $v\wedge Y_1\wedge\ldots\wedge Y_k=0$. Further, a point of $\mathbb{P}\big(\bigwedge^k\mathbb{C}^n\big)$ is in the image of p if and only if its representation as a linear combination of the basis elements of $\bigwedge^k\mathbb{C}^n$, consisting of all possible distinct wedge products of a k-dimensional basis in $\mathbb{C}^n$, is completely decomposable. Hence the image of p is a subvariety of $\mathbb{P}\big(\bigwedge^k\mathbb{C}^n\big)$ of completely decomposable elements. It can also be realized as follows. A natural coordinatization of $\mathbb{P}\big(\bigwedge^k\mathbb{C}^n\big)$ is through the determinants of all the $k\times k$ minors of Y, normalized by a chosen minor characterized by an index $\mathfrak{i}$, hence $\mathbb{P}\big(\bigwedge^k\mathbb{C}^n\big)\cong\mathbb{P}^{\binom{n}{k}-1}$. These minor determinants—the Plücker coordinates—are not all independent, indeed, they satisfy quadratic relations known as the *Plücker relations* (which may themselves not all be independent). The image of the Plücker map p is thus the subspace of $\mathbb{P}^{\binom{n}{k}-1}$ cut out by the quadratic Plücker relations.

3. Grassmannian flows

3.1. **Tangent space decomposition.** Recall that we can consider the Stiefel manifold as a fibre bundle $\mathbb{V}(n,k)=\mathrm{Gr}(n,k)\times\mathrm{GL}(k)$. Our goal here is to characterize the induced decomposition of the tangent space $\mathrm{T}_Y\mathbb{V}(n,k)$ for $Y\in\mathbb{V}(n,k)$. We can decompose the tangent space $\mathrm{T}_Y\mathbb{V}(n,k)$ into horizontal and vertical subspaces (see, for example, Montgomery [76, p. 149])

$$\mathrm{T}_Y\mathbb{V}(n,k)=\mathbb{H}_Y\oplus\mathbb{V}_Y\,.$$

The horizontal subspace $\mathbb{H}_Y$ is associated with the tangent space of the Grassmannian base space, while the vertical subspace $\mathbb{V}_Y$ is associated with the fibres homeomorphic to $\mathrm{GL}(k)$. Let us choose the coordinate patch representation $\mathbb{U}_\mathfrak{i}$ for $\mathrm{Gr}(n,k)$ for some $\mathfrak{i}=\{i_1,\dots,i_k\}\subset\{1,\dots,n\}$. Let $P_\mathfrak{i}$ denote the projection matrix of size $n\times n$ that contains zeros everywhere except at positions (i_l,i_l) for $l=1,\dots,k$ where it contains ones. Note that one can additively decompose any given tangent vector $V=P_\mathfrak{i}V+P_{\mathfrak{i}^\circ}V$. Hence we have

$$\begin{aligned}\mathbb{H}_Y&=\big\{P_{\mathfrak{i}^\circ}V\colon V\in\mathrm{T}_Y\mathbb{V}(n,k)\big\}\cong\mathbb{C}^{(n-k)k}\,,\\ \mathbb{V}_Y&=\big\{P_\mathfrak{i}V\colon V\in\mathrm{T}_Y\mathbb{V}(n,k)\big\}\cong\mathfrak{gl}(k)\,.\end{aligned}$$

3.2. **Fibre bundle flow.** Suppose we are given a vector field on the Stiefel manifold

$$V(x,Y) = A(x,Y)\,Y,$$

for any $(x,Y) \in \mathbb{R} \times \mathbb{V}(n,k)$ where $A \in \mathfrak{gl}(n)$. Fixing a coordinate patch $\mathbb{U}_{\mathfrak{i}}$ for $\mathrm{Gr}(n,k)$ for some $\mathfrak{i} = \{i_1, \dots, i_k\}$ we can always decompose $Y \in \mathbb{V}(n,k)$ into

$$Y = y_{\mathfrak{i}^\circ}\, u_{\mathfrak{i}}.$$

Let a, b, c and d denote the $\mathfrak{i} \times \mathfrak{i}$, $\mathfrak{i} \times \mathfrak{i}^\circ$, $\mathfrak{i}^\circ \times \mathfrak{i}$ and $\mathfrak{i}^\circ \times \mathfrak{i}^\circ$ minors of A, respectively.

Theorem 1. *The flow governed by $V(x,Y)$ generates a coupled flow in $\mathrm{Gr}(n,k) \times \mathrm{GL}(k)$ for $Y = y_{\mathfrak{i}^\circ} u_{\mathfrak{i}}$, where for a given fixed $\mathfrak{i}$, the flow in the coordinate chart variables $\hat{y} = \varphi_{\mathfrak{i}} \circ y_{\mathfrak{i}^\circ}$ and the flow of rank k transformations $u_{\mathfrak{i}}$ are governed by*

$$\hat{y}' = c + d\,\hat{y} - \hat{y}(a + b\,\hat{y}) \qquad \text{and} \qquad u_{\mathfrak{i}}' = (a + b\,\hat{y})\,u_{\mathfrak{i}},$$

where we now think of a, b, c and d as functions of x, $u_{\mathfrak{i}}$ and $\hat{y}$.

Proof. Using that $Y = y_{\mathfrak{i}^\circ} u_{\mathfrak{i}}$ the ordinary differential system $Y' = V(x,Y)$ becomes

$$y_{\mathfrak{i}^\circ}' u_{\mathfrak{i}} + y_{\mathfrak{i}^\circ} u_{\mathfrak{i}}' = (A_{\mathfrak{i}} + A_{\mathfrak{i}^\circ} y_{\mathfrak{i}^\circ})\, u_{\mathfrak{i}},$$

where $A_{\mathfrak{i}}$ represents the minor obtained by restricting the matrix $A(x, y_{\mathfrak{i}^\circ} u_{\mathfrak{i}})$ to its $\mathfrak{i}$th columns. Applying the projections $P_{\mathfrak{i}}$ and $P_{\mathfrak{i}^\circ}$ to both sides of this equation, respectively generates the equations for $u_{\mathfrak{i}}$ and $\hat{y}$ shown. Note that $\hat{y}$ is the projection of $y_{\mathfrak{i}^\circ}$ onto its $\mathfrak{i}^\circ$th rows, as well as its image under the coordinate chart $\varphi_{\mathfrak{i}}$. □

3.3. **Riccati flow.** A natural decoupling of the flow on the base space $\mathrm{Gr}(n,k)$ from the flow on the fibres $\mathrm{GL}(k)$ occurs when the vector field V is linear, i.e. when

$$V(x,Y) = A(x)\,Y,$$

The following corollary is immediate from Theorem 1.

Corollary 1. *If the vector field V is linear so that $A = A(x)$ only, then:*

1. *The flow on the base space $\mathrm{Gr}(n,k)$ decouples from the flow evolving through the fibres $\mathrm{GL}(k)$—the flow in the fibres is slaved to that in the base space;*
2. *For a fixed coordinate patch $\mathbb{U}_{\mathfrak{i}}$ index by $\mathfrak{i}$, in the coordinate chart variables $\hat{y} = \varphi_{\mathfrak{i}} \circ y_{\mathfrak{i}^\circ}$, the flow is governed by the Riccati differential system:*

$$\hat{y}' = c(x) + d(x)\hat{y} - \hat{y}a(x) - \hat{y}b(x)\hat{y}.$$

Suppose we are required to determine the flow generated by a linear nonautonomous vector field defined on the Stiefel manifold $\mathbb{V}(n,k)$. The first conclusion in the corollary implies that all the relevant information is carried in the flow in the Grassmann manifold $\mathrm{Gr}(n,k)$, and the flow through the fibres $\mathrm{GL}(k)$ can be completely determined a-posteriori from the Grassmannian flow. The second conclusion suggests that if we fix a coordinate patch, then the flow in the Grassmannian can be determined from the solution to the Riccati system for $\hat{y}$. If required, we can solve the differential system for $u_{\mathfrak{i}}$ in Theorem 1 to determine Y, thereby completely resolving the flow generated by the linear vector field V on the Stiefel manifold. Provided $\hat{y}$ remains finite, this approach in fact works.

The problem is that, though $Y = y_{\mathfrak{i}^\circ} u_{\mathfrak{i}}$ must be globally finite as it is generated by a linear vector field (with globally smooth coefficients), the Riccati solution $\hat{y}$ itself can become singular in a finite integration interval. Of course simultaneously the determinant of $u_{\mathfrak{i}}$ itself becomes zero. The solution on the Grassmannian does

not become singular. The issue is representation. (Note that the flow on $\mathrm{GL}(k)$ is linear but rank is not preserved because its coefficients depend on the Riccati flow.)

The Riccati flow is a flow in a given fixed coordinate chart indexed by $\mathfrak{i}$, which is chosen at the start of integration. Given an initial element in $\mathbb{V}(n,k)$, we pick a (good) coordinate patch $\mathbb{U}_\mathfrak{i}$ for $\mathrm{Gr}(n,k)$, this fixes the Grassmannian representation $y_{\mathfrak{i}^\circ}$. Projecting onto the $\mathfrak{i}^\circ$th rows of $y_{\mathfrak{i}^\circ}$, or equivalently looking at the image under the coordinate chart $\varphi_\mathfrak{i}$, generates $\hat{y} \in \mathbb{C}^{(n-k)k}$. The Riccati flow is the flow in the Euclidean chart image space $\mathbb{C}^{(n-k)k}$. Each coordinate patch $\mathbb{U}_\mathfrak{i}$ is dense in $\mathrm{Gr}(n,k)$. Therefore in numerical computations, the Riccati solution $\hat{y}$ is likely to leave and return to the patch $\mathbb{U}_\mathfrak{i}$ across any discrete integration step that staddles a representation singularity (generating a large but finite solution $\hat{y}$ the other side).

With this in mind, Schiff and Shnider [90] suggested the following method that integrates through singularities in the Riccati flow. Fix a coordinate patch $\mathbb{U}_\mathfrak{i}$ with index $\mathfrak{i}$. The general linear group $\mathrm{GL}(n)$ acts transitively on $\mathbb{V}(n,k)$ (and also $\mathrm{Gr}(n,k)$): the left Lie group action $\Lambda\colon \mathrm{GL}(n) \times \mathbb{V}(n,k) \to \mathbb{V}(n,k)$ is defined by $\Lambda\colon (S,Y) \mapsto SY$. For $Y_0 \in \mathbb{V}(n,k)$ we set

$$\Lambda_{Y_0}\colon S \mapsto S\,Y_0.$$

The Möbius Lie group action $\mu_{\hat{y}_0}\colon \mathrm{GL}(n) \to \mathbb{C}^{(n-k)k}$ is defined by $\mu_{\hat{y}_0}\colon S \mapsto \varphi_\mathfrak{i} \circ \pi_\mathfrak{i} \circ \Lambda_{\varphi_\mathfrak{i}^{-1}\circ\hat{y}_0} \circ S$, where $\pi_\mathfrak{i}\colon \mathbb{V}(n,k) \to \mathbb{U}_\mathfrak{i}$ is the quotient map $\pi_\mathfrak{i}\colon Y \mapsto y_{\mathfrak{i}^\circ}$. Explicitly, if $S_{\mathfrak{i},\mathfrak{i}'}$ represents the $\mathfrak{i} \times \mathfrak{i}'$ minor of S, we have:

$$\mu_{\hat{y}_0}\colon S \mapsto (S_{\mathfrak{i},\mathfrak{i}} + S_{\mathfrak{i},\mathfrak{i}^\circ}\hat{y}_0)(S_{\mathfrak{i}^\circ,\mathfrak{i}} + S_{\mathfrak{i}^\circ,\mathfrak{i}^\circ}\hat{y}_0)^{-1}.$$

Thus, given data $\hat{y}_0$ in the Euclidean chart image space $\mathbb{C}^{(n-k)k}$, pullback to the Lie group $\mathrm{GL}(n)$, to the identity element I_n, using the Möbius Lie group action map $\mu_{\hat{y}_0}$. Advance the solution across one integration step in the Lie group generating the element $S \in \mathrm{GL}(n)$. Schiff and Shnider used a Neumann/Runge–Kutta method to do this, but a Lie group method could also be used. Now push forward to $\hat{y} = \mu_{\hat{y}_0} \circ S \in \mathbb{C}^{(n-k)k}$ using the Möbius Lie group action map. This takes you back to the chart corresponding to the original coordinate patch $\mathbb{U}_\mathfrak{i}$.

This method integrates through singularities in the Riccati flow. However, we are still left with another associated practical problem. If the linear vector field V depends on a parameter we wish to vary, the singularities in the Riccati flow can drift in the domain of integration and impinge on the matching position.

4. Practical Grassmann integration

Our goal in this section is construct numerical methods that integrate the flow associated with the push forward of the linear vector field V onto the Grassmannian manifold, whilst avoiding the representation singularities that occur in the Riccati approach. The solution is to change patch continuously in some optimal fashion or whenever the coordinate patch becomes a poor representation.

The following diagram helps map out the two new strategies we suggest.

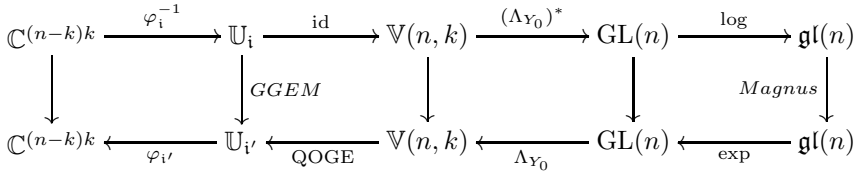

4.1. **Continuous optimal patch evolution.** The idea behind the *Grassmann Gaussian elimination method* (GGEM) is this. Given data in $\mathrm{Gr}(n,k)$ that lies in a given patch $Y_0 \in \mathbb{U}_{\mathfrak{i}}$ identified by $\mathfrak{i}$, pullback to the Stiefel manifold using the identity map—note $\mathbb{U}_{\mathfrak{i}} \subset \mathbb{V}(n,k)$—so $Y_0 \in \mathbb{V}(n,k)$. Advance the solution one integration step along the Stiefel manifold $\mathbb{V}(n,k)$, using say a classical Runge–Kutta method, thus generating the element $Y \in \mathbb{V}(n,k)$.

Now with the next step solution on the Stiefel manifold, we use *quasi-optimal Gaussian elimination* with partial pivoting (QOGE) to decompose $Y = y_{(\mathfrak{i}')^\circ} u_{\mathfrak{i}'}$ and project onto the coordinate patch $\mathbb{U}_{\mathfrak{i}'}$ producing the element $y_{(\mathfrak{i}')^\circ} \in \mathbb{U}_{\mathfrak{i}'}$. The quasi-optimal Gaussian elimination process (described in Section 5) picks out a suitable coordinate patch $\mathbb{U}_{\mathfrak{i}'}$ to represent the solution, which may be different than the original patch $\mathbb{U}_{\mathfrak{i}}$.

To ensure we numerically remain with the Stiefel manifold, rather than use a Runge–Kutta method, we might use a Lie group method as follows (see Munthe–Kaas [77]). Pullback the data $Y_0 \in \mathbb{V}(n,k)$ from the Stiefel manifold to the general linear group $\mathrm{GL}(n)$, via the action map Λ_{Y_0}. The corresponding element in $\mathrm{GL}(n)$ is naturally the identity element I_n. Subsequently pullback, via the exponential map, to the zero element in the corresponding Lie algebra, i.e. $\mathsf{o} \in \mathfrak{gl}(n)$. Evolve the solution on the Lie algebra to $\sigma \in \mathfrak{gl}(n)$ using the Magnus expansion (Magnus [68]; also see Iserles, Munthe–Kaas, Nørsett and Zanna [54]). Pushforward from $\mathfrak{gl}(n)$ to $\mathrm{GL}(n)$, via the exponential map, producing the Lie group element $S = \exp\sigma \in \mathrm{GL}(n)$. Now pushfoward to the Stiefel manifold $\mathbb{V}(n,k)$ via the Lie group action map Λ_{Y_0}. For more details on Lie group methods for Stiefel manifolds, see Krogstad [61] and Celledoni and Owren [20].

4.2. **Riccati flow with patch swapping.** Since we are interested in constructing the flow generated by the push forward of the vector field V onto the Grassmann manifold, we can avoid singularities in any given Riccati system chart flow associated with a given Grassmannian coordinate patch, by simply changing patch when the solution representation appears to become poor. In particular, we could either change the coordinate patch when the:

- Norm $\|\hat{y}\|_\infty$ becomes too large (the easier and preferred approach we take);
- Determinant $\det u_{\mathfrak{i}}$ becomes too small (this involves constructing $u_{\mathfrak{i}}$ as integration proceeds and we want to avoid carrying information unnecessarily).

Hence if say $\|\hat{y}\|_\infty$ exceeds a prescribed tolerance at the end of one step, to change patch, we apply the quasi-optimal Gaussian elimination method (QOGE) to the matrix $y_{\mathfrak{i}^\circ} = \varphi_{\mathfrak{i}}^{-1} \circ \hat{y}$. This identifies a new patch and index $\mathfrak{i}'$ to use for the next set of successive steps until $\|\hat{y}\|_\infty$ becomes too large again, and so forth.

4.3. **Drury–Oja flow.** There is a close connection between the Riccati flow in Corollary 1 and the continuous orthogonalization method of Humpherys and Zumbrun [49], proved by direct comparison.

Lemma 1. *If $\hat{y} \in \mathbb{C}^{(n-k)k}$ satisfies the Riccati flow $\hat{y}' = c(x) + d(x)\hat{y} - \hat{y}a(x) - \hat{y}b(x)\hat{y}$ and $u \in \mathbb{U}(k)$ satisfies $u' = -\hat{y}^\dagger(c + d\,\hat{y})\,u$, then for any index $\mathfrak{i}$, we have that $Q = y_{\mathfrak{i}^\circ} u$ satisfies the Drury–Oja flow: $Q' = (I_n - QQ^\dagger)AQ$.*

Humpherys and Zumbrun [49] derive this flow by a QR-decomposition of the solution $Y = QR \in \mathbb{V}(n,k)$ to the linear, spectral, globally bounded flow $Y' = A(x)\,Y$.

We can think of this continuous orthogonalization method as generating an approximate flow on the Grassmann manifold whilst evolving the coordinatization (see Edelman, Arias and Smith [33]; Bindel, Demmel and Friedman [11]). It is also known as a Drury–Oja flow (see Drury [32], Oja [80], Yan, Helmke and Moore [97], Bridges and Reich [15], Dieci and Van Vleck [30] and Hairer, Lubich and Wanner [42, p. 136]). The determinant of the upper triangular matrix, $\det R$, grows exponentially. Thus, since it is nonzero in the far field, we know it remains nonzero in the whole integration interval $\mathbb{R}$. Consequently, $Q = YR^{-1}$ is globally finite on $\mathbb{R}$, i.e. there are no singularities in the Drury–Oja flow.

There is a natural $\mathfrak{su}(n)$ Lie algebra action on the Stiefel manifold of orthonormal k-frames, $\mathbb{V}_0(n,k)$, generated by the map $(\sigma, Q) \mapsto \exp(\sigma)\, Q$, for $Q \in \mathbb{V}_0(n,k)$ and $\sigma \in \mathfrak{su}(n)$. If $v \circ Q \equiv (I - QQ^\dagger)\, A$, the flow on the Lie algebra $\mathfrak{su}(n)$ that generates the Drury–Oja flow on $\mathbb{V}_0(n,k)$ is governed by $\sigma' = \operatorname{dexp}_\sigma^{-1} \circ v\big(\exp(\sigma) Q_0\big)$. We could use this to construct a numerical method that preserves orthonormality of Q.

5. Grassmann Gaussian elimination method

5.1. **Algorithm.** The *Grassmann Gaussian elimination method* using a Lie group method on the Stiefel manifold (GGEM-LG), proceeds as follows:

(1) Suppose initially we are given data $y_{\mathtt{i}_m^\circ}(x_m)$ in the coordinate patch $\mathbb{U}_{\mathtt{i}_m}$.
(2) Across the integration interval $[x_m, x_{m+1}]$, compute σ_m using the Magnus expansion—we recommend the fourth order Magnus expansion that includes the first commutation term.
(3) Compute $Y_{m+1} = \exp \sigma_m \cdot y_{\mathtt{i}_m^\circ}(x_m)$.
(4) Apply the quasi-optimal Gaussian elimination (QOGE) algorithm (outlined below) to Y_{m+1}; this generates the solution $y_{\mathtt{i}_{m+1}^\circ}(x_{m+1})$ in the coordinate chart $\mathbb{U}_{\mathtt{i}_{m+1}}$.

Across the integration interval $[x_m, x_{m+1}]$, we could generate Y_{m+1} from $y_{\mathtt{i}_m^\circ}(x_m)$ by solving the flow on the Stiefel manifold $\mathbb{V}(n,k)$ using a classical Runge–Kutta step (GGEM-RK). Both algorithms are summarized in the following diagram.

$$
\begin{array}{ccccccc}
y_{\mathtt{i}_m^\circ}(x_m) & \xrightarrow{\ \mathrm{id}\ } & y_{\mathtt{i}_m^\circ}(x_m) & \xrightarrow{(\Lambda_{y_{\mathtt{i}_m^\circ}(x_m)})^*} & I_n & \xrightarrow{\ \log\ } & \mathfrak{o} \\
\big\downarrow{\scriptstyle GGEM} & & \big\downarrow{\scriptstyle RK} & & & & \big\downarrow{\scriptstyle Magnus} \\
y_{\mathtt{i}_{m+1}^\circ}(x_{m+1}) & \xleftarrow[\ \mathrm{QOGE}\ ]{} & Y_{m+1} & \xleftarrow[\Lambda_{y_{\mathtt{i}_m^\circ}(x_m)}]{} & S_m & \xleftarrow[\ \exp\ ]{} & \sigma_m
\end{array}
$$

5.2. **Quasi-optimal Gaussian elimination.** To project the endpoint solution Y_{m+1} in the Stiefel manifold onto a quasi-optimal coordinate patch, say $\mathbb{U}_{\mathtt{i}_{m+1}}$, we use a Gauss–Jordan approach. This entails using elementary column operations and *optimal pivoting*, until a specified $k \times k$ minor of Y_{m+1} becomes the identity matrix. To be more explicit about what we mean by optimal pivoting, we outline the procedure:

(1) Look for the largest term in magnitude in $Y^{(1)} = Y_{m+1}$. Nominate this term as the pivot term and suppose this occurs in row i_1, column j_1.
(2) Use elementary column operations with this term, $Y^{(1)}_{i_1,j_1}$, as the pivot to render all other terms in that row zero. Finally, use the elementary column operation of scalar multiplication to render the pivot term itself equal to one.

We have thus performed the decomposition (see for example Meyer [73])

$$Y^{(1)} = Y^{(2)}\, L_1,$$

where the elementary column operations performed are encoded in the elementary matrix L_1, with $\det L_1 = Y^{(1)}_{i_1,j_1}$. The resulting matrix $Y^{(2)}$ has value one at position (i_1, j_1) and otherwise zeros in row i_1.

(3) In the $n \times (k-1)$ minor of $Y^{(2)}$ identified by the columns $\{1,\dots,k\}\backslash\{j_1\}$, look for the largest term in magnitude. Again nominate this term as the pivot term and suppose this occurs in row i_2 (which will be distinct from i_1), column j_2. Here j_2 refers to the column relative to the original $n \times k$ matrix $Y^{(2)}$, and which, by choice of the minor is distinct from j_1.

(4) Use elementary column operations with this term, $Y^{(2)}_{i_2,j_2}$, as the pivot to render all other terms in that row of the minor of $Y^{(2)}$ equal to zero. Again use the elementary column operation of scalar multiplication to render the pivot term itself equal to one. We have thus performed the decomposition

$$Y^{(2)} = Y^{(3)}\, L_2,$$

where the elementary column operations performed are encoded in the elementary matrix L_2, with $\det L_2 = Y^{(1)}_{i_2,j_2}$. The matrix $Y^{(3)}$ has value one at positions (i_1, j_1) and (i_2, j_2), and otherwise zeros in rows i_1 and i_2.

(5) Continue this process, looking at the $n \times (k-2)$ minor of $Y^{(3)}$ with columns $\{1,\dots,k\}\backslash\{j_1, j_2\}$ and so forth, up to and including the kth step. We then perform column *swaps* to ensure that the $\mathfrak{i} \times \{1,\dots,k\}$ minor of final matrix is the identity matrix. These column swaps can be encoded in the elementary matrix Σ, with $\det \Sigma = (-1)^{\#\{\text{swaps}\}}$. This process generates a matrix decomposition, with $\mathfrak{i} = \{i_1,\dots,i_k\}$, of the form:

$$Y_{m+1} = y_{\mathfrak{i}\circ}\, L,$$

where $L = \Sigma \cdot L_k \cdots L_1 \in \mathrm{GL}(k)$, with

$$\det L = (-1)^{\#\{\text{swaps}\}}\, Y^{(k)}_{i_k,j_k} \cdots Y^{(2)}_{i_2,j_2} Y^{(1)}_{i_1,j_1}.$$

The question is how much information in L do we need to retain at each step? This arises because the linear vector field will typically depend analytically on some parameters, in particular the spectral parameter. We want the flow we construct from the Grassmannian flow to also depend analytically on such parameters.

Theorem 2. *The entries of $y_{\mathfrak{i}\circ}$ and L, generated by the elementary column operations just described, are finite. Further, the product $(\det L)\, y_{\mathfrak{i}\circ}$ depends analytically on the elements of Y_{m+1}.*

Proof. First we focus on the application of the Grassmann Gaussian elimination method to Y_{m+1}—whose columns are linearly independent. We need to show that each term in the scalar prefactor product $Y^{(k)}_{i_k,j_k} \cdots Y^{(2)}_{i_2,j_2} Y^{(1)}_{i_1,j_1}$ is non-zero and finite. The first element $Y^{(1)}_{i_1,j_1}$ must be finite as it is a component in the solution of a linear system of equations (with a bounded coefficient matrix). It must be nonzero as it is the largest element in magnitude in Y_{m+1} (and we assume a nontrivial solution). The element $Y^{(2)}_{i_2,j_2}$ must also be finite, as it is produced by a single elementary column operation with divisor $Y^{(1)}_{i_1,j_1}$. It must be nonzero as it is the largest element in the minor constructed by missing out the i_1th row and the columns of that

minor must be linearly independent. We iterate this argument to the kth step. That the products of the scalar prefactor product $Y^{(k)}_{i_k,j_k} \cdots Y^{(2)}_{i_2,j_2} Y^{(1)}_{i_1,j_1}$ with each of the entries of $y_{\mathrm{i}\circ}$ depend analytically on the elements of Y_{m+1} follows naturally from the fact that the divisors in each of the elementary column operations performed, are present in the scalar prefactor. □

Corollary 2. *The Grassmann Gaussian elimination method, which numerically approximates the flow generated by the push forward to the Grassmann manifold* $\mathrm{Gr}(n,k)$ *of a linear vector field on the Stiefel manifold* $\mathbb{V}(n,k)$*, generates a numerical flow on the product space*

$$\mathrm{Gr}(n,k) \otimes \mathbb{C},$$

which retains any analytic dependence on parameters inherited by the linear vector field on the Stiefel manifold $\mathbb{V}(n,k)$*.*

The column swaps encoded in the elementary matrix Σ are not strictly necessary. We include them to be consistent with our choice of representative patch—we chose a covering class characterized by the property that a given $k \times k$ minor is the identity matrix. We could generalize the matrix representation for patches of $\mathrm{Gr}(n,k)$ to include $n \times k$ matrices with a $k \times k$ minor which is a rank k multiple of the identity matrix. An example would be the matrix $Y^{(k)}$ in the quasi-optimal Gaussian elimination process we describe above, *before* we perform column swaps.

5.3. **Complexity.** The complexity of the quasi-optimal Gaussian elimination algorithm, dominated by the search for the largest elements in the successively decreasing minors $Y^{(i)}$ of Y_{m+1}, is of order nk^2. The method is a practical approach to maximize the determinant of the $k \times k$ minor removed from Y_{m+1}. It will not in general choose the minor with the largest determinant—hence the label *quasi-optimal*. This could be achieved by searching through all the $k \times k$ minors of Y_{m+1}, i.e. all the Plücker coordinates, but this has complexity of order n choose k. Perhaps there is an efficient way to use the Plücker relations to reduce this complexity?

6. Spectral problems

6.1. **Linear Stiefel flow.** Consider the linear spectral problem on $\mathbb{R}$:

$$Y' = A(x;\lambda)\, Y$$

We assume there exists a subdomain $\Omega \subseteq \mathbb{C}$ containing the right-half complex plane, such that for $\lambda \in \Omega$ there exists exponential dichotomies on $\mathbb{R}^-$ and $\mathbb{R}^+$ with the same Morse index k in each case (see Henry [43] and Sandstede [88]). Let $Y^-(x;\lambda) \in \mathbb{V}(n,k)$ denote the matrix whose columns are solutions to the spectral problem and which span the unstable manifold section at $x \in [-\infty,+\infty)$. Let $Y^+(x;\lambda) \in \mathbb{V}(n,n-k)$ denote the matrix whose columns are the solutions which span the stable manifold section at $x \in (-\infty,+\infty]$.

6.2. **Matching.** The values of spectral parameter $\lambda \in \Omega$ for which the columns of Y^- and columns of Y^+ are linearly dependent on $\mathbb{R}$ are pure-point eigenvalues. The *Evans function* $D(\lambda)$ is the measure of the degree linear dependence between the two basis sets Y^- and Y^+, i.e. of the degree of transversal intersection between the unstable and stable manifolds (see Alexander, Gardner and Jones [2]; Nii [79]):

$$D(\lambda) \equiv \mathrm{e}^{-\int_0^x \mathrm{Tr} A(\xi;\lambda)\,\mathrm{d}\xi} \det\bigl(Y^-(x;\lambda)\ Y^+(x;\lambda)\bigr).$$

In practice we drop the analytic, non-zero, scalar exponential prefactor and evaluate the Evans function at a matching point x_*. Further, for Y^- and Y^+ we need only retain the information carried in their Grassmannian projections (together with a complex scalar multiplicative factor encoding the patch-to-patch transformations). As described above, this is because the linear flow through the fibres $\mathrm{GL}(k)$ is completely determined by the flow on the Grassmann manifold $\mathrm{Gr}(n,k)$. The rank of the flow through the fibres is maintained and therefore the determinant of the solution $u_{\mathfrak{i}}$ is non-zero, provided the coefficients of the linear flow remain finite. The flow induced through the fibres $\mathrm{GL}(k)$, by either the GGEM or Riccati flow with patch swapping methods, guarantee this. If we substitute the decompositions $Y^{\pm} = y_{\mathfrak{i}^{\pm}} u_{\mathfrak{i}^{\pm}}$ into the determinant in the Evans function above, then we can re-write the Evans function as $\det\big(y_{\mathfrak{i}^-}(x_*;\lambda)\ y_{\mathfrak{i}^+}(x_*;\lambda)\big)$ multipled by the scalar factors $\det u_{\mathfrak{i}^-}$ and $\det u_{\mathfrak{i}^+}$ (both of which we drop henceforth). For GGEM and the Riccati flow with patch swapping, we record in $\det L^{\pm}(x_*;\lambda)$ the accumulated elementary column operations that describe patch changes and alter the determinant of the Evans function. Hence we evaluate the modified Evans function

$$D(\lambda;x_*) \equiv \det L^-(x_*;\lambda)\cdot\det L^+(x_*;\lambda)\cdot\det\big(y_{\mathfrak{i}^-}(x_*;\lambda)\ y_{\mathfrak{i}^+}(x_*;\lambda)\big).$$

There are other matching criteria measuring the degree of intersection between subspaces that do not use the determinant: for example computing the angle between subspaces as suggested by Björck and Golub [13] or computing the smallest eigenvalue as suggested by Hutson [51] and Ixaru [55]. Both these latter techniques might be important for large systems when computing the determinant could be an unstable process, indeed, we investigate them in this context in Ledoux, Malham, Niesen and Thümmler [66]. However in both cases the magnitude of a function of the spectral parameter is computed, whose zeros correspond to eigenvalues. Hence we must search for touchdowns to zero in the complex parameter spectral plane which can be problematic. For the examples we consider here, which are not too large, using the determinant suffices.

6.3. **Initialization.** We construct the $n\times k$ matrix $Y_0^-(\lambda)$ whose columns are the k eigenvectors of $A(-\infty;\lambda)$ corresponding to eigenvalues with a positive real part (see Humpherys and Zumbrun [49] and also Humpherys, Sandstede and Zumbrun [50] for how to preserve analyticity with respect to the spectral parameter λ). We then simply perform quasi-optimal Gaussian elimination on $Y_0^-(\lambda)$; this automatically chooses a suitable initial coordinate patch $\mathbb{U}_{\mathfrak{i}}$ and initial data to start the GGEM. In practice, integration starts at $x=\ell_-$ for some suitable, usually negative, value of ℓ_-. Analogously we construct the $n\times(n-k)$ matrix $Y_0^+(\lambda)$ whose columns are the $n-k$ eigenvectors of $A(+\infty;\lambda)$ corresponding to eigenvalues with a negative real part. Again we perform quasi-optimal Gaussian elimination and integrate backwards from $x=\ell_+$ for some suitable, usually large and positive, value of ℓ_+.

6.4. **Scaled GGEM.** From Theorem 2 we know that the numerical flow generated by the Grassmann Gaussian elimination method is globally finite and $\det L\cdot y_{\mathfrak{i}^\circ}$ is analytic in the spectral parameter. In practice with GGEM, in each integration step we store $\det L$ as a complex scalar, along with the matrix $y_{\mathfrak{i}^\circ}$. In fact we simply update $\det L$ by the values $Y^{(l)}_{i_l,j_l}$ for $l=1,\ldots,k$ and any sign changes due to column swaps as we proceed through the quasi-optimal Gaussian elimination process. We update $\det L$ and $y_{\mathfrak{i}^\circ}$ separately at each successive step, combining them at the end of the last integration step. The scalar prefactor represents the determinant

of the $k \times k$ minor we have extracted at each step and grows exponentially. This would be tempered by the scalar exponential prefactor in the definition of the Evans function. An accurate practical procedure here is as follows. When integrating in the interval $[\ell_-, x_*]$, at each step, divide the scalar factor resulting from GGEM by $\exp\big((\mu_1^-(\lambda)+\cdots+\mu_k^-(\lambda))h\big)$, where h is the stepsize, and the $\mu_i^-(\lambda)$ are the (spatial) eigenvalues, with positive real part, of $A(-\infty;\lambda)$. When integrating in the interval $[\ell_+, x_*]$, at each step, divide the scalar factor by $\exp\big(-(\mu_1^+(\lambda)+\cdots+\mu_{n-k}^+(\lambda))h\big)$, where the $\mu_i^+(\lambda)$ are the eigenvalues, with negative real part, of $A(+\infty;\lambda)$.

To see that this normalization is appropriate, we recall the Plücker coordinates of Section 2. After applying the optimal Gaussian elimination algorithm to Y_{m+1} the $\mathfrak{i}^\circ$th row elements of $y_{\mathfrak{i}^\circ}$ are themselves $(n-k)k$ Plücker coordinates; normalized by $\det L$. The $\mathfrak{i}^\circ$th row elements of $\det L \cdot y_{\mathfrak{i}^\circ}$ and $\det L$, can be used to reconstruct the remaining Plücker coordinates through the homogeneous, quadratic Plücker relations. Hence the Plücker coordinates, or complete set of $k \times k$ minors, of Y_{m+1} and $y_{\mathfrak{i}^\circ}$ differ by a factor $\det L$. It is well known that if the original vector field on $\mathbb{V}(n,k)$ is linear, then the Plücker coordinates corresponding to Y_{m+1} satisfy a (larger) linear system of equations. In the left far field the coordinates thus grow exponentially, in fact with growth rate $\mu_1^-(\lambda)+\cdots+\mu_k^-(\lambda)$; hence our recommendation to divide by the exponential factor suggested (with an analogous argument for the right far field). See Alexander, Gardner and Jones [2], Alexander and Sachs [3], Brin [16, 17] or Allen and Bridges [5] for more details.

7. Applications

We present some numerical results for three different applications. The three applications reduce to the solution of a system showing multiple distinct exponential growth and decay rates in the stable and unstable subspaces, respectively. We show that our approach resolves this numerical obstacle successfully and can compete with the continuous orthogonalization method of Humpherys and Zumbrun [49].

7.1. **Algorithms.** We implement six different algorithms as follows.

(1) Riccati-RK: Riccati method with fixed coordinatization with the flow of the Riccati vector field approximated by the classical fourth order Runge–Kutta method. We generically chose the coordinatization labelled by $\mathfrak{i}^- = \{1,\dots,k\}$ and $\mathfrak{i}^+ = \{k+1,\dots,n\}$ for the left-hand and right-hand intervals, respectively. Hence if $Y_0^-(\lambda)$ and $Y_0^+(\lambda)$ denote the unstable and stable subspaces of $A(-\infty;\lambda)$ and $A(+\infty;\lambda)$, respectively, then we set

$$\hat{y}^\pm(\ell_\pm;\lambda) = \big(Y_0^\pm(\lambda)\big)_{(\mathfrak{i}^\pm)^\circ,\mathfrak{i}^\pm}\big(Y_0^\pm(\lambda)\big)^{-1}_{\mathfrak{i}^\pm,\mathfrak{i}^\pm},$$

where $(Y)_{\mathfrak{i},\mathfrak{i}'}$ denotes the $\mathfrak{i} \times \mathfrak{i}'$ minor of Y. We integrate the Riccati equation outlined in Corollary 1 in the two intervals and evaluate the modified Evans function

$$D(\lambda;x_*) \equiv \det\begin{pmatrix} I_k & \hat{y}^+(x_*;\lambda) \\ \hat{y}^-(x_*;\lambda) & I_{n-k} \end{pmatrix}.$$

Provided neither Riccati flow becomes singular, this Evans function is analytic in the spectral parameter λ.

(2) Möbius–Magnus: Uses the Schiff and Shnider approach to integrate through singularities, combined with a Lie group method to advance the solution on the general linear group, as described at the end of Section 3. The same generic fixed

coordinate charts are used as for the Riccati-RK method above. Over the integration interval $[x_m, x_{m+1}]$ with an equidistant mesh stepsize h, we advance the solution on the Lie algebra using the fourth order Magnus method

$$\sigma_m = \tfrac{1}{2}h\big(A(x_m^{[1]}) + A(x_m^{[2]})\big) - \tfrac{\sqrt{3}}{12}h^2\big[A(x_m^{[1]}), A(x_m^{[2]})\big],$$

with the two Gauss–Legendre points (see Iserles, Marthinsen and Nørsett [52])

$$x_m^{[1]} = x_m + (\tfrac{1}{2} - \tfrac{1}{6}\sqrt{3})h \quad \text{and} \quad x_m^{[2]} = x_m + (\tfrac{1}{2} + \tfrac{1}{6}\sqrt{3})h.$$

We then compute the Möbius map $\hat{y}_{m+1} = \mu_{\hat{y}_m} \circ \exp \sigma_m$ to advance the solution in the fixed Grassmannian chart—for the left-hand interval $\mathfrak{i}^- = \{1, \dots, k\}$ while for the right-hand interval $\mathfrak{i}^+ = \{k+1, \dots, n\}$. We evaluate the same Evans function as for the Riccati-RK method above.

(3) GGEM-RK: Scaled Grassmann Gaussian elimination method, with the classical fourth order Runge–Kutta method used to advance the solution on the Stiefel manifold, as described in Sections 5 and 6.4. We evaluate the modified Evans function in Section 6.

(4) GGEM-LG: Same as GGEM-RK but with a fourth order Magnus method used to advance the solution on the Stiefel manifold instead, i.e. $Y_{m+1} = \exp(\sigma_m)\, y_{\mathfrak{i}_m}$ where σ_m is generated as for the Möbius–Magnus method above.

(5) Riccati-QOGE: Riccati method with coordinate swapping as described in Section 4.2. We have chosen to implement the method in the following form. At each integration step we advance the solution on the Stiefel manifold using the Magnus method (we could also use a Runge–Kutta method here). We apply elementary column operations to the resulting solution matrix to convert the pre-determined rows indexed by $\mathfrak{i}$ from the previous step to the identity matrix. Then if $\|\hat{y}\|_\infty$ is less than or equal to a tolerance size, we keep this index $\mathfrak{i}$ for the next step. If it is greater, we apply QOGE at the end of the next step after advancing the solution on the Stiefel manifold, thus generating a new index. As for GGEM-RK and GGEM-LG, we update $\det L$ at each step (produced by the elementary column operations with the pre-determined index or QOGE). We divide $\det L$ by the scalar exponential factors, as described for the scaled GGEM method. We evaluate the same modified Evans function also.

(6) CO-RK: Continuous orthogonalization method of Humpherys and Zumbrun with the classical fourth order Runge–Kutta method used to advance the solution on the Stiefel manifold of orthonormal frames. The initial conditions $Q_0^\pm(\lambda)$ for the Q-matrices are obtained by QR-factorization of $Y_0^\pm(\lambda)$. From Humpherys and Zumbrun [49], to ensure analyticity we must also solve the scalar problems $(\det R^\pm)' = \operatorname{Tr}\big(Q^\dagger A(x;\lambda)Q - (Q_0^\pm(\lambda))^\dagger A(\pm\infty;\lambda)Q_0^\pm(\lambda)\big)\det R^\pm$. The Evans function is then given by

$$D(\lambda; x_*) = \det R^-(x_*;\lambda)\cdot \det R^+(x_*;\lambda)\cdot \det\big(Q^-(x_*;\lambda)\ Q^+(x_*;\lambda)\big).$$

7.2. **Boussinesq system.** As the first test system, we consider the Boussinesq system studied by Humpherys and Zumbrun [49]. The (good) Boussinesq equation, expressed in a co-moving frame moving to the right with wave speed c, is given by

$$u_{tt} = (1-c^2)\,u_{xx} + 2c\,u_{xt} - u_{xxxx} - (u^2)_{xx}.$$

It has solitary wave solutions of the form $\bar{u}(x) \equiv \frac{3}{2}(1-c^2)\operatorname{sech}^2\big(\frac{1}{2}\sqrt{1-c^2}\,x\big)$, where $|c| < 1$. These waves are stable when $1/2 < |c| < 1$ and unstable when $|c| < 1/2$.

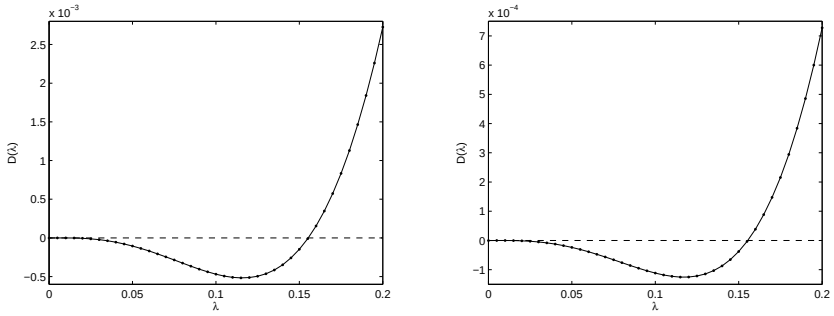

FIGURE 1. The Evans function of the Boussinesq system for the unstable pulse having wave speed $c = 0.4$. The left plot is generated by the Riccati-RK method with fixed coordinate patches identified by $\mathfrak{i}^- = \{1, 2\}$ over $[-8, 0]$ and $\mathfrak{i}^+ = \{3, 4\}$ over $[0, 8]$. The right plot shows the result of the CO-RK method.

TABLE 1. Zero of the Evans function for the Boussinesq problem computed with the Riccati-RK method (with fixed coordinate patches identified by $\mathfrak{i} =^- \{1, 2\}$ over $[-8, 0]$ and $\mathfrak{i}^+ = \{3, 4\}$ over $[0, 8]$) and the CO-RK method. Here N is the number of (equidistant) steps used in the mesh.

N	Riccati-RK	CO-RK
128	0.15544090	0.15540090
256	0.15543184	0.15542952
512	0.15543143	0.15543129
1024	0.15543141	0.15543140
2048	0.15543141	0.15543141
4096	0.15543141	0.15543141

If we consider small perturbations about the travelling wave $\bar{u}$ we generate a linear spectral problem of the form $Y' = A(x; \lambda)Y$, where

$$A(x;\lambda) = \begin{pmatrix} 0 & 1 & 0 & 0 \\ 0 & 0 & 1 & 0 \\ 0 & 0 & 0 & 1 \\ -\lambda^2 - 2\bar{u}'' & 2\lambda c - 4\bar{u}' & (1-c^2) - 2\bar{u} & 0 \end{pmatrix}.$$

When the spectral parameter λ lies in the right-half complex plane the eigenvalues of $A(\pm\infty; \lambda)$ spectrally separate into two growth and two decay modes, i.e. $k = 2$. We used $\ell_\pm = \pm 8$ in our experiments.

In Figure 1 we show the Evans function computed along the real axis from $\lambda = 0$ to $\lambda = 0.2$ for the unstable pulse with $c = 0.4$. The Riccati-RK (left plot) and CO-RK (right plot) methods detect a zero of the Evans function near $\lambda = 0.155$, indicating an unstable eigenvalue there. An accurate value of the eigenvalue can be found by using a standard root-finding method. This yields the values in Table 1. The Riccati-RK and the CO-RK methods both converge to the same eigenvalue when the number of steps N increases. As a check, the Matlab `ode45`

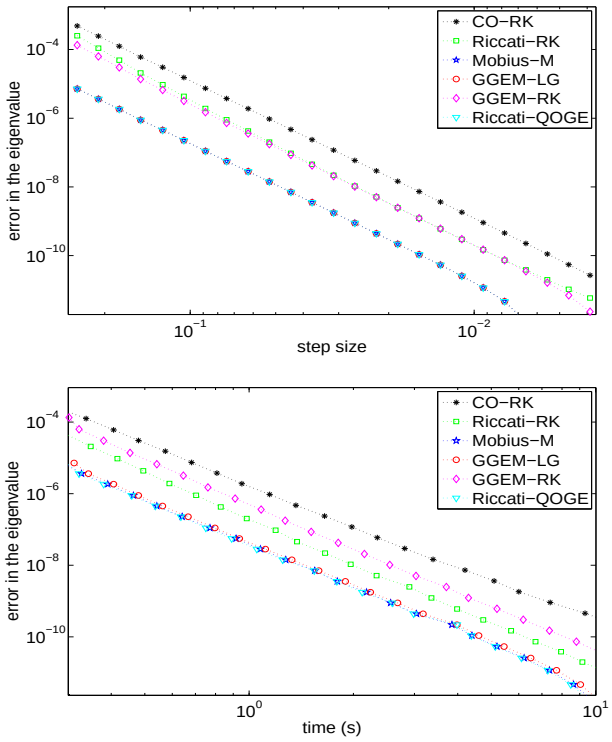

FIGURE 2. Error in the eigenvalue, vs stepsize (upper panel) and vs cputime (lower panel), matching at $x_* = 0$.

solver was used with a relative tolerance 10^{-8} and absolute tolerance 10^{-10} to integrate the systems, leading to the same resulting eigenvalue: $\lambda = 0.15543141$ for both methods.

Function evaluation for the Riccati vector field requires three matrix-matrix multiplications. This is the same number of matrix-matrix multiplications needed to evaluate the Drury–Oja vector field. However, the matrices in the Drury–Oja vector field are $n \times k$ and $n \times (n-k)$, respectively, while the matrices in the Riccati vector fields have smaller dimension: $(n-k) \times k$. Because of the smaller dimension of the systems to be integrated, our Riccati approach is faster than the continuous orthogonalization problem. For example, to construct Figure 1 the Evans function was evaluated at 200 distinct λ values between $\lambda = 0$ and $\lambda = 0.2$. Using the fourth-order Runge-Kutta method with $N = 512$ steps, this required 33 seconds for the CO-RK method, while the Riccati-RK method needed 24 seconds (Matlab-implementation, CPU 2.4GHz).

In Figure 2 we compare the error in the eigenvalue and efficiency of computation for all six methods, when we match at $x_* = 0$. We see that the methods that use the Magnus expansion to advance the solution on the Stiefel manifold are the most accurate for a given stepsize. They are also the most efficient, delivering the best accuracy for given computational effort. The Riccati-RK method does not suffer from singularities for the chosen fixed patches when matching at $x_* = 0$, at least for

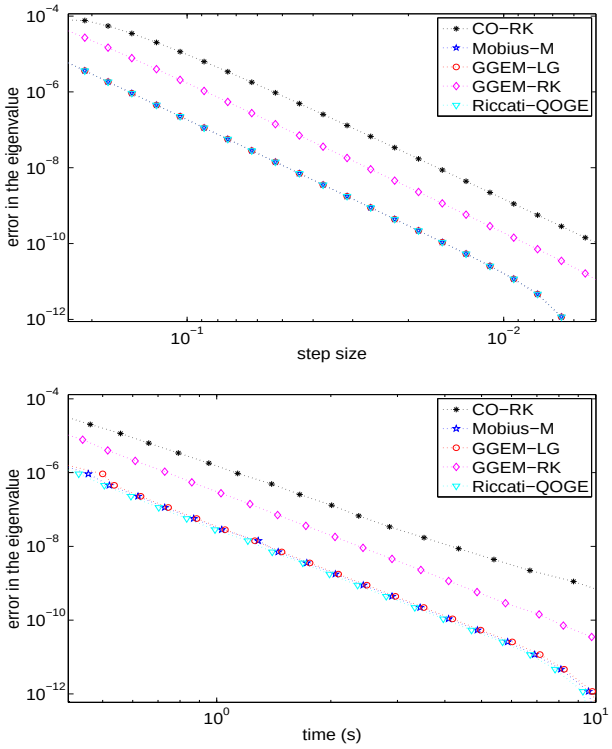

FIGURE 3. Error in the eigenvalue vs stepsize (upper panel) and vs cputime (lower panel), matching at $x_* = 8$.

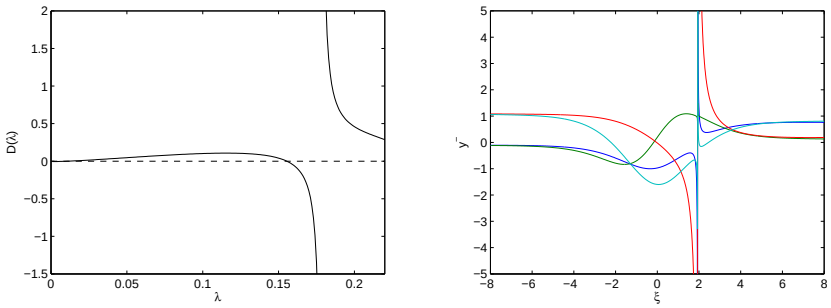

FIGURE 4. The Evans function when the Möbius–Magnus method is applied (left panel) with the matching point as $x_* = +8$. The entries of the solution $\hat{y}^-$, passing through the singularity when integrating from -8 to 8, for $\lambda = 0.15543141$ (right panel).

the range of values of the spectral parameter in the vicinity of the eigenvalue (as well as the origin and anywhere inbetween). However, if we change the matching point to $x_* = \ell_+ = +8$ there are singularities in the Riccati-RK solution (as a result of a vanishing determinant of u_{i-}). In particular, a singularity appears around $x = 2$

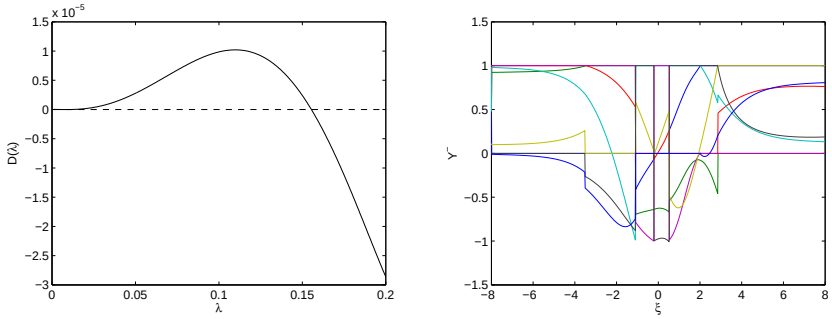

FIGURE 5. The Evans function which results when the GGEM-RK scheme is applied over $[-8, 8]$, matching point in $x_* = 8$ (left panel). The entries of y_i for $\lambda = 0.15543141$ (right panel).

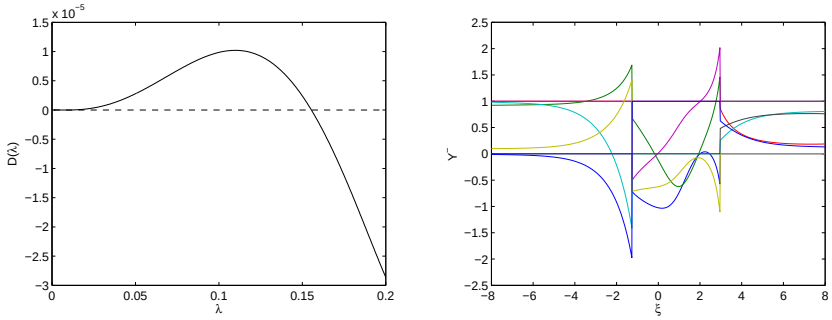

FIGURE 6. The Evans function when the Riccati-QOGE method is applied (left panel). The entries of $\hat{y}^-$ are shown for $\lambda = 0.15543141$ (right panel). The criterion used for swapping to a new coordinate patch was $\|\hat{y}^-\|_\infty > 2$.

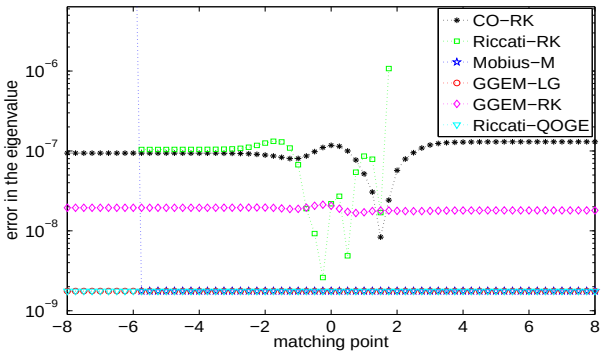

FIGURE 7. Error in the eigenvalue for different choices of the matching point. The number of steps in the equidistant mesh was $N = 512$.

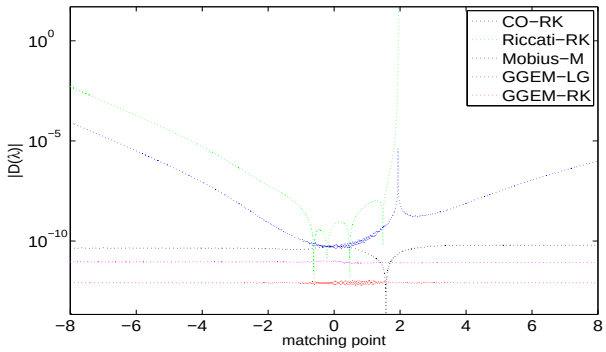

FIGURE 8. $|D(\lambda)|$ for λ equal to the eigenvalue for different matching points. The number of steps in the equidistant mesh was $N = 512$.

for λ equal to the eigenvalue (see Figure 4). Hence we compare the remaining five methods in Figure 3 in this case. We see that using the Möbius–Magnus method to integrate through a singularity does not introduce loss in accuracy. The resulting Evans function can have poles, as seen in Figure 4, which appear at λ-values where the Riccati equation has a singularity at the matching point. This means that in some cases the matching point should be chosen rather carefully in order not to have the poles interfering with the eigenvalue(s). When applying GGEM-RK the Evans function is analytic and the choice of the matching point is less important.

Figure 5 shows the Evans function obtained when the GGEM-RK evolves y_{i} from $\ell_- = -8$ to $\ell_+ = +8$. To construct the plot in Figure 5, the quasi-optimal Gaussian elimination process was applied at each step in the integration. However it is clear from the right plot in Figure 5, that multiple successive steps can be integrated in the same coordinate patch. For example, between $x = -8$ and $x = -3$ the coordinate patch does not change. Performing the whole quasi-optimal Gaussian elimination process only when a certain criterion is satisfied, reduces the computing time. Using the Riccati-QOGE method, we change the coordinatization when $\|\hat{y}^-\|_\infty > 2$. This generates an Evans function very similar to that in Figure 5. As seen in Figure 6 the quasi-optimal Gaussian elimination process is then performed only two times for λ equal to the eigenvalue.

We compare the error in computing the eigenvalue for different choices of matching point—in fact for x_* anywhere in the interval $[-8, 8]$—for all six methods in Figure 7. We see that the most accurate and robust methods are the GGEM-LG and Riccati-QOGE methods. Some methods, such as the Riccati-RK method as discussed already, break down when singularities impinge on the matching point—the singularities in the Evans function are observed in Figure 8. Generally we also see in Figure 7 that the GGEM-LG and Riccati-QOGE methods outperform the CO-RK method in terms of accuracy.

Overall, we observe in this example that when computing the eigenvalue, those methods based on the Magnus expansion are superior in accuracy and efficiency. Note that for GGEM-RK, the quasi-optimal Gaussian elimination process is an additional nk^2 operation. However, to ensure analyticity for the CO-RK method,

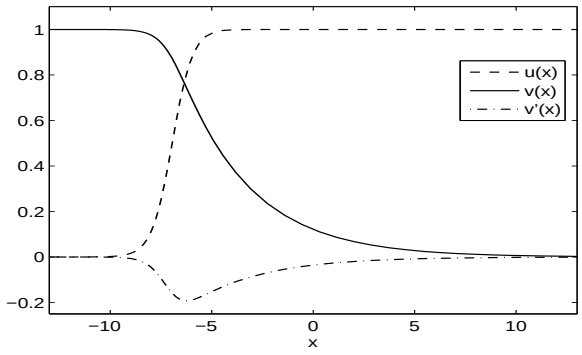

FIGURE 9. The travelling wave solution for $\delta = 0.1$ and $m = 9$.

there are two additional matrix-matrix multiplications in the equations for $\det R^{\pm}$ (operational cost kn^2) required at each step.

7.3. **Autocatalytic fronts.** As a second example, we study travelling waves in a model of autocatalysis in an infinitely extended medium

$$u_t = \delta u_{xx} + cu_x - uv^m,$$
$$v_t = v_{xx} + cv_x + uv^m.$$

Here $u(x,t)$ is the concentration of the reactant and $v(x,t)$ is the concentration of the autocatalyst. We suppose (u,v) approaches the stable homogeneous steady state $(0,1)$ as $x \to -\infty$, and the unstable homogeneous steady state $(1,0)$ as $x \to +\infty$. The diffusion parameter δ is the ratio of the diffusivity of the reactant to that of the autocatalyst and m is the order of the autocatalytic reaction. The speed of the co-moving reference frame is c. The system is globally well-posed for smooth initial data and any finite $\delta > 0$ and $m \geq 1$.

From Billingham and Needham [9] we know that a unique heteroclinic connection between the unstable and stable homogeneous steady states exists for wavespeeds $c \geq c_{\min}$. The unique travelling wave for $c = c_{\min}$ converges exponentially to the homogeneous steady states and is computed by a simple shooting algorithm (see Balmforth, Craster and Malham [8]). The resulting travelling wave for $\delta = 0.1$ and $m = 9$ is shown in Figure 9.

The stability of the travelling wave of velocity c can be deduced from the location of the spectrum of the eigenvalue problem $Y' = A(x;\lambda)Y$, where

$$A(x;\lambda) = \begin{pmatrix} 0 & 0 & 1 & 0 \\ 0 & 0 & 0 & 1 \\ \lambda/\delta + \bar{v}^m/\delta & m\bar{u}\bar{v}^{m-1}/\delta & -c/\delta & 0 \\ -\bar{v}^m & \lambda - m\bar{u}\bar{v}^{m-1} & 0 & -c \end{pmatrix},$$

where $\bar{u}$ and $\bar{v}$ represent the travelling wave solution.

The pulsating instability occurs when $\delta < 1$ is sufficiently small and m is sufficiently large (see Metcalf, Merkin and Scott [72] and Balmforth, Craster and Malham [8]). For δ fixed and m increasing, a complex conjugate pair of eigenvalues crosses into the right-half λ-plane signifying the onset of instability via a Hopf bifurcation. Figure 10 shows the onset of this instability for $\delta = 0.1$ as m is

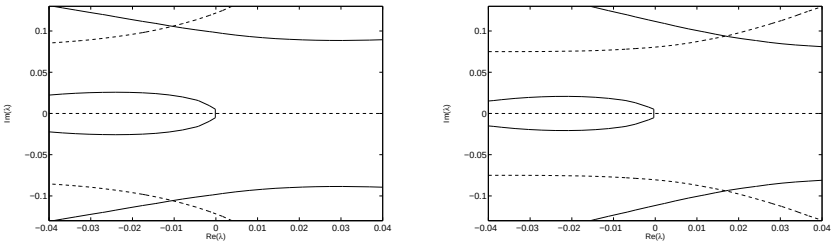

FIGURE 10. Zero contour lines of the real (solid) and imaginary (dashed) parts of the Evans function for the autocatalysis problem with $\delta = 0.1$ and $m = 8$ (left panel) and $m = 9$ (right panel).

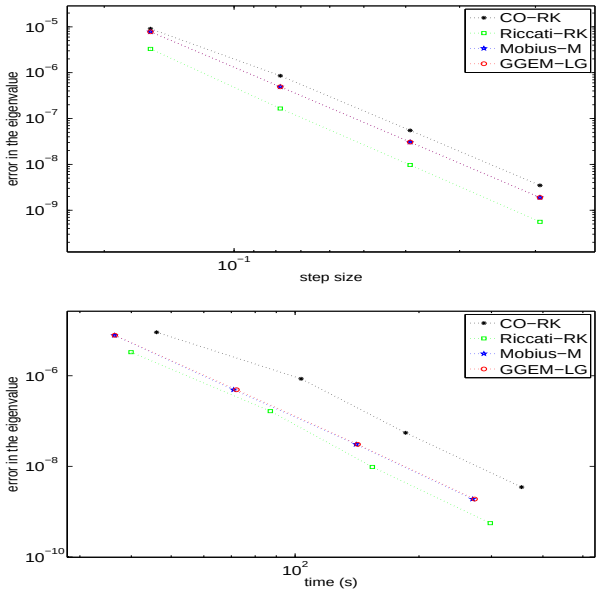

FIGURE 11. Error in the eigenvalue in the first quadrant when $\delta = 0.1$ and $m = 9$ for different methods, vs stepsize (upper panel) and vs cputime (lower panel), matching at $x_* = 0$.

increased from 8 to 9 (see Aparicio, Malham and Oliver [7]). The figure shows the zero contour lines of the real and imaginary parts of the Evans function. Solid lines correspond to zero contours of the real part of $D(\lambda)$, dashed lines to the imaginary part of $D(\lambda)$. We see that a complex-conjugate pair of eigenvalues crosses into the right-half plane, indicating the onset of instability. Figure 10 was constructed using the Riccati-RK method with the fixed coordinate patches identified by $\mathfrak{i}^- = \{1, 2\}$ from $x = -10$ to $x_* = -7$, and $\mathfrak{i}^+ = \{3, 4\}$ from $x = 10$ to $x_* = -7$. The matching point $x_* = -7$ is chosen roughly centred on the wavefront.

We compare the Riccati-RK, Möbius–Magnus, CO-RK and GGEM-LG methods in Figure 11 where we plot the absolute error in the eigenvalue vs the stepsize (upper panel) and also vs cputime (lower panel). The eigenvalue in question is that in the

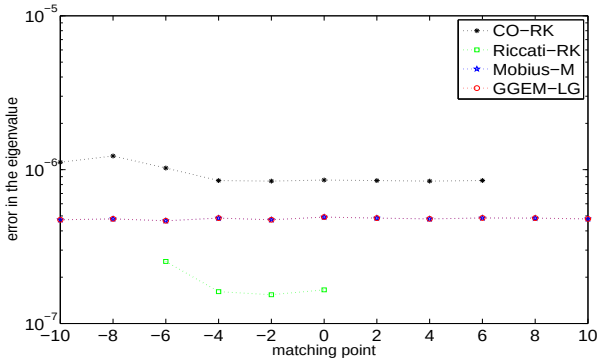

FIGURE 12. Error in the eigenvalue in the first quadrant when $\delta = 0.1$ and $m = 9$, for different methods, for different matching points. The number of steps in the equidistant mesh is $N = 256$.

first quadrant in Figure 10 for $\delta = 0.1$ and $m = 9$. Figure 11 was generated as follows. Starting with an initial guess lying within a small square around the eigenvalue, we iterated a standard root finding algorithm until we arrived in a square (containing the eigenvalue) which was smaller than a preset tolerance. We see in Figure 11 that the Riccati-RK method produces a slightly better error for a given stepsize, and is marginally more efficient than the GGEM-LG method. The CO-RK method produces a larger error for a given computational effort. This is not surprising, as again, the matrices in the Drury–Oja vector field are twice as big (4×2) as the ones in the Riccati vector fields (2×2).

When we match at $x_* = -7$, there is little to distinguish the Riccati-RK, Möbius–Magnus, CO-RK and GGEM-LG methods. We compare all four methods for different matching positions x_* in Figure 12, which was generated using the same root finding criteria as for Figure 11, except all the methods used $N = 256$ steps. Note that the errors in the Möbius–Magnus and GGEM-LG methods are uniform for any matching values in the range $[-10, 10]$. The CO-RK method error doesn't vary that much either and is slightly larger. Note that no values are plotted for the CO-RK method at the matching points $x_* = 8, 10$. In these cases the classical Runge–Kutta method applied to the Drury–Oja vector field is unstable for $N = 256$ steps for some λ-values close to the eigenvalue. This problem is resolved by increasing the number of steps to $N = 512$. For a range of matching positions roughly in $[-10, 0]$, there are no singularities of the Riccati-RK method in the left and right-hand integration intervals for values of the spectral parameter λ close to the eigenvalue. Indeed for this range of matching positions the Riccati-RK method delivers the best accuracy. However for matching positions outside this range, for values of the spectral parameter λ not far from the eigenvalue, the Riccati-RK solution does have a singularity for some matching points (which we can see in the contour plots in Figure 13). This makes the eigenvalue-searching algorithm fail—indicated by no error points for those matching position values. We also do not show the error for the Riccati-RK method for the matching points $x_* = -8, -10$, as there are singularities in the Evans function close to the real axis for these matching points (again see Figure 13). This means that we cannot for example, apply

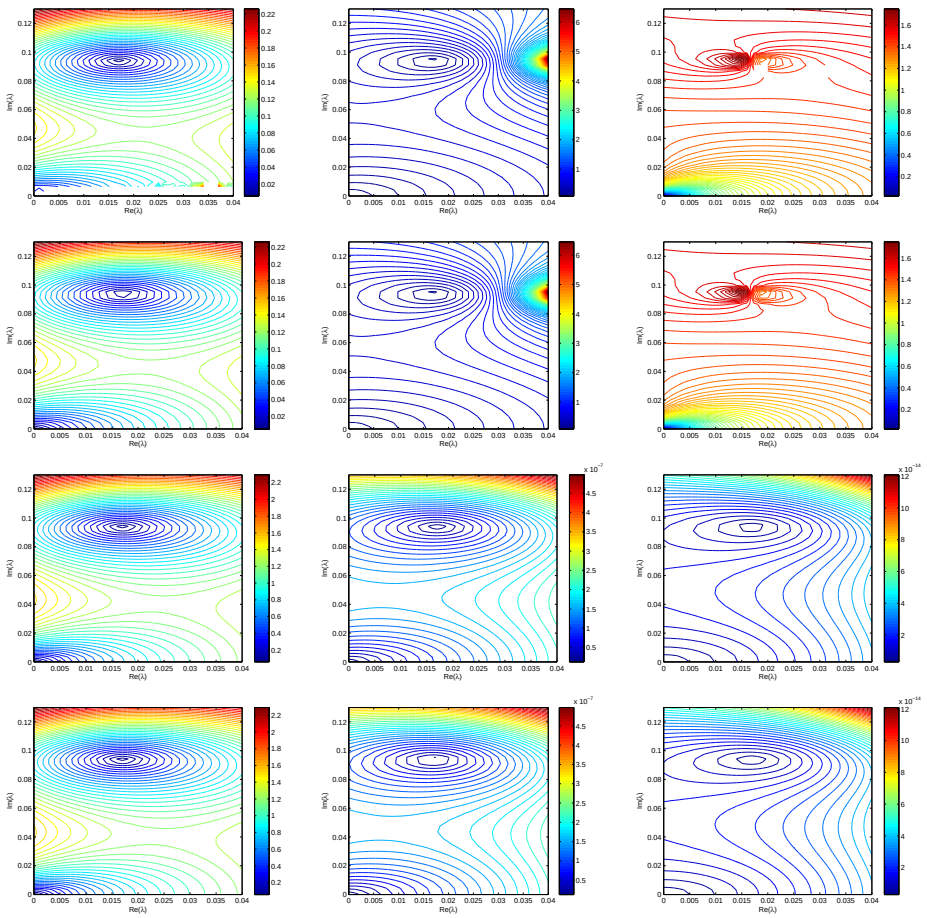

FIGURE 13. Contour lines of $|D(\lambda)|$ for $\delta = 0.1$ and $m = 9$ when using the Riccati-RK, Möbius–Magnus, CO-RK and GGEM-LG methods (order: top three down to bottom three), matching at positions $x_* = -8, 0, +8$ (left to right).

the argument principle in the first quadrant, though starting sufficiently close to the eigenvalue we can still use the Riccati-RK method as part of a root-finding algorithm to determine the eigenvalue.

Figure 13 shows the contour lines of $|D(\lambda)|$ for $\delta = 0.1$ and $m = 9$, close to the eigenvalue in the first quadrant, when using the Riccati-RK, Möbius-Magnus, CO-RK and GGEM-LG methods, respectively, and matching at three positions $x_* = -8, 0, +8$. We see that the CO-RK and GGEM-LG methods show the least sensitivity to the choice of matching position and produce smooth contour plots for all three matching points. The contour plots across shape and scale look very similar for both these methods. By contrast the Riccati-RK and Möbius-Magnus methods develop singularities close to the eigenvalue when the matching position x_* is 0 or $+8$.

7.4. **Ekman boundary layer.** The third test system is a boundary layer flow over a flat plate which is infinitely extended in the x and y direction and rotates around the half infinite z-axis with a given rotational speed. Linear stability of the Ekman boundary layer has been investigated in Allen and Bridges [6] and Allen [4] using the compound matrix method. The flow is governed by the continuity equation $u_x + v_y + w_z = 0$, and the Navier-Stokes equations in a co-rotating frame

$$\begin{aligned} u_t + uu_x + vu_y + wu_z + \tfrac{1}{\mathrm{R_o}}p_x - \tfrac{2}{\mathrm{R_o}}v &= \tfrac{1}{\mathrm{R_e}}(u_{xx} + u_{yy}) + \tfrac{1}{\mathrm{R_o}}u_{zz}, \\ v_t + uv_x + vv_y + wv_z + \tfrac{1}{\mathrm{R_o}}p_y + \tfrac{2}{\mathrm{R_o}}u &= \tfrac{1}{\mathrm{R_e}}(v_{xx} + v_{yy}) + \tfrac{1}{\mathrm{R_o}}v_{zz}, \\ w_t + uw_x + vw_y + ww_z + \tfrac{1}{\mathrm{R_o}\mathrm{E_k}}p_z &= \tfrac{1}{\mathrm{R_e}}(w_{xx} + w_{yy}) + \tfrac{1}{\mathrm{R_o}}w_{zz}. \end{aligned}$$

Here $\mathrm{R_e}$, $\mathrm{R_o}$ and $\mathrm{E_k}$ denote the Reynolds, Rossby and Ekman numbers, respectively.

After non-dimensionalization and setting $\mathrm{R_e} = \mathrm{R_o}$, $\mathrm{E_k} = 1$, the linear stability of the boundary layer is determined by the eigenvalues λ of the linear problem $Y' = A(z;\lambda)Y$, where (see Allen [4, p. 176])

$$A(z;\lambda) = \begin{pmatrix} 0 & 1 & 0 & 0 & 0 & 0 \\ 0 & 0 & 1 & 0 & 0 & 0 \\ 0 & 0 & 0 & 1 & 0 & 0 \\ -a(z,\lambda) & 0 & b(z,\lambda) & 0 & 0 & -2 \\ 0 & 0 & 0 & 0 & 0 & 1 \\ i\gamma\mathrm{R_e}V_z(z) & 2 & 0 & 0 & b(z,\lambda) - \gamma^2 & 0 \end{pmatrix}$$

and

$$\begin{aligned} V(z) &= \cos(\epsilon)\big(1 - \exp(-z)\cos(z)\big) + \sin(\epsilon)\exp(-z)\sin(z), \\ V_z(z) &= \exp(-z)\big(\sin(z+\epsilon) + \cos(z+\epsilon)\big), \\ U(z) &= -\sin(\epsilon)\big(1 - \exp(-z)\cos(z)\big) + \cos(\epsilon)\exp(-z)\sin(z), \\ U_{zz}(z) &= -2\exp(-z)\cos(z+\epsilon), \\ a(z,\lambda) &= \gamma^4 + i\mathrm{R_e}\gamma^2\big(\gamma U(z) - i\lambda\big) + i\gamma\mathrm{R_e}U_{zz}(z), \\ b(z,\lambda) &= 2\gamma^2 + \mathrm{R_e}\big(i\gamma U(z) + \lambda\big). \end{aligned}$$

Here the parameters γ and ϵ represent the radial and angle components, respectively, of a polar coordinate parameterization of horizontal wavenumbers associated with the x and y directions—see Allen and Bridges [6] for more details.

We choose the fixed coordinate patch identified by $\mathfrak{i}^+ = \{1,2,3\}$ to integrate the corresponding Riccati equation from $z = \ell_+$ to $z_* = 0$. The boundary condition for the rigid wall at $z_* = 0$ as given in Allen and Bridges is

$$Y_1(0;\lambda) = Y_2(0;\lambda) = Y_5(0;\lambda) = 0.$$

If

$$Y^- = \begin{pmatrix} 1 & 0 & 0 & 0 & 0 & 0 \\ 0 & 1 & 0 & 0 & 0 & 0 \\ 0 & 0 & 0 & 0 & 1 & 0 \end{pmatrix},$$

then the boundary conditions are equivalent to

$$\det\big(Y^- \cdot Y^+(0;\lambda)\big) = 0\,.$$

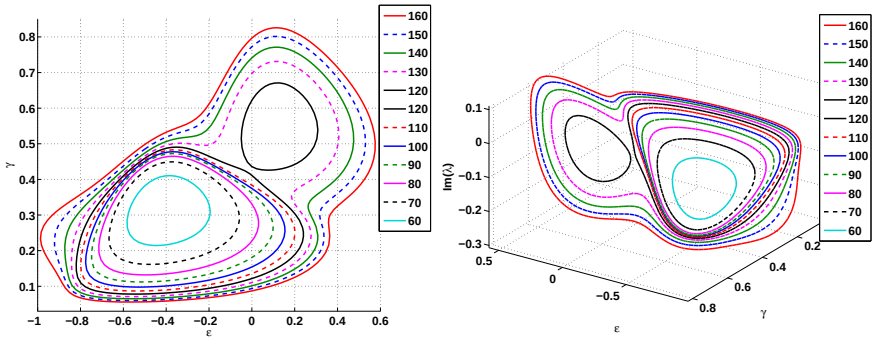

FIGURE 14. Neutral curves for rigid wall, $\mathrm{R_e}$ fixed (values indicated).

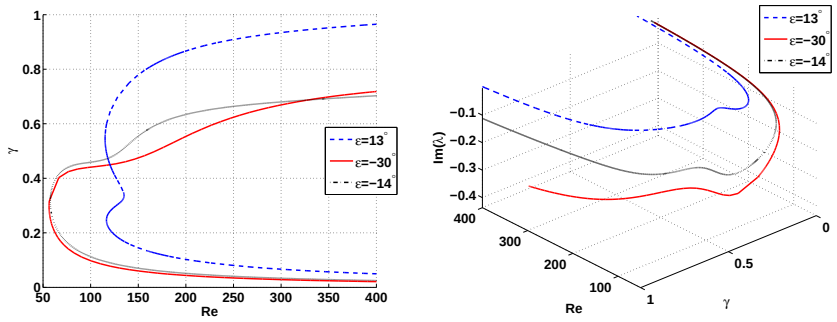

FIGURE 15. Neutral curves for rigid wall, ϵ fixed.

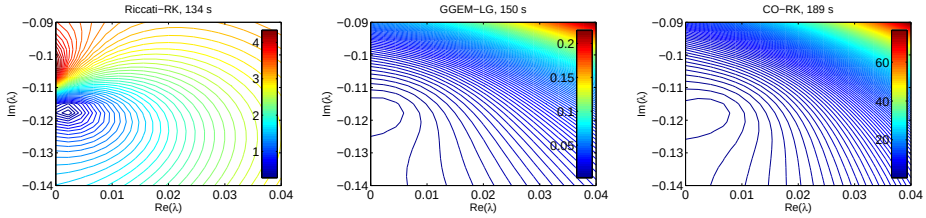

FIGURE 16. Contour plots of $|D(\lambda;0)|$ for $\mathrm{R_e} = 140$, $\epsilon = 0.014156$, $\gamma = 0.70575$. An equidistant mesh was used with 500 intervals and values computed on a 20×20 grid in the complex λ-plane.

We thus compute the Evans function:

$$D(\lambda; z_*) = \det\left(Y^- \cdot \begin{pmatrix} I \\ \hat{y} \end{pmatrix}\right) = \det \begin{pmatrix} 1 & 0 & 0 \\ 0 & 1 & 0 \\ \hat{y}_{21} & \hat{y}_{22} & \hat{y}_{23} \end{pmatrix} \equiv \hat{y}_{23}(z_*; \lambda).$$

We computed neutral curves, i.e. curves in the ϵ–γ plane where $Re(\lambda) = 0$, using the Riccati-RK method with $\mathfrak{i}^+ = \{1, 2, 3\}$ to compute $\hat{y}(0;\lambda) \in \mathbb{C}^{3\times 3}$ and consequently the Evans function $D(\lambda; z_*)$. For continuation of the curves we used the Matlab package MatCont which uses pseudo-arclength continuation (Dhooge,

Govaerts and Kuznetsov [29]). Figures 14 and 15 show the neutral curves which match those in Allen and Bridges [6] and Allen [4]. The integration of the Riccati system has been done with the Matlab ODE-solver `ode23s` from $z = 10$ to $z_* = 0$ (as in Allen and Bridges) with absolute and relative tolerances 10^{-6} and 10^{-4}. The stable subspace of $A(+\infty;\lambda)$ was constructed using the Matlab eigenvalue-solver `eig` (we also used direct formulae for the eigenvectors to construct analytic bases for the stable subspace but this did not significantly change the overall performance).

For comparison we also implemented the CO-RK and GGEM-LG methods. We tested the performance of all three methods, in each case evaluating the Evans function on a 20×20 grid for λ in the complex plane. In Figures 16 we present contour plots of $|D(\lambda;0)|$, and see that all methods find a root at $\lambda \approx 0.002 - 0.117\mathrm{i}$. The computation times for a 2.4Ghz machine were: 134 seconds for Riccati-RK, 150 seconds for GGEM-LG and 189 seconds for CO-RK. As a comprehensive check, we also implemented the compound matrix method (i.e. Plücker coordinates, of which there are 20), described in Allen and Bridges, for this performance test. As expected, since this method involves integrating a linear system of order 20, it was an order of magnitude slower (while giving the same results).

8. Concluding discussion

We have shown that the new scaled Grassmann Gaussian elimination method as well as the Riccati method with quasi-optimal patch swapping, compete with the continuous orthogonalization method for computing the Evans function. Both new methods deliver superior accuracy for the same computational cost when combined with Lie group Magnus integration to advance the solution. Moreover, as hoped, numerically these new methods appear to be robust in the sense that they are insensitive to the choice of the matching position in the computational domain. We now outline several directions in which we plan to use these methods as well as extend them.

One of the main goals we have had in mind in this paper is that of large scale spectral problems, in particular the stability of travelling waves with a multi-dimensional structure. There is recent research extending the Evans function approach in this direction—see Deng and Nii [27], Gesztesy, Latushkin and Makarov [36] and Gesztesy, Latushkin and Zumbrun [37]. From a numerical perspective we have, together with Niesen, implemented some of the methods we propose in this paper in a multi-dimensional context. In particular, it is well known in autocatalysis and combustion that planar travelling fronts can be unstable to transverse perturbations and develop into steadily propagating travelling fronts with wrinkles. In Ledoux, Malham, Niesen and Thümmler [66] we show that the wrinkled fronts themselves develop an instability as a diffusion parameter is further increased.

For large scale problems the Lie group methods we propose using the Magnus expansion may become prohibitive. This is because of the effort required to compute the matrix exponential—see Moler and Van Loan [75], Celledoni and Iserles [19], Munthe-Kaas and Zanna [78] and Iserles and Zanna [53]. For the examples we considered this was not an issue. However it remains to be seen if such Lie group methods will be cost effective for larger problems—the methods we proposed based on Runge–Kutta integration such as GGEM-RK can be used as they scale favourably with system size.

The constructs and Grassmannian reductions we have considered in this paper, it turns out, have their origins in the control theory literature dating back to the early seventies, in particular in the pioneering papers of Hermann and Martin [44, 45, 46, 47, 48], Martin and Hermann [71] and Brockett and Byrnes [18]. We also found Bittanti, Laub and Willems [12], Lafortune and Winternitz [63], Rosenthal [87], Shayman [91] and Zelikin [99] particularly useful resources. A future direction we would like to explore is whether there are any applications of the numerical methods we have outlined here to practical non-autonomous control problems?

Riccati methods in particular also have their origins in the quantum chemistry literature also dating back to the early seventies—a recent survey of these numerical methods can be found in Chou and Wyatt [24]. However also see Light and Walker [67], Johnson [56], Hutson [51] and Gray and Manopoulous [39]. In particular the log-derivative and R-propagation methods correspond to special choices of Grassmannian patch in the Riccati methods we mention above. Prüfer methods, for which we can think of the patch evolving, originate even further back; see Prüfer [84] and Pryce [85].

Of course, our quasi-optimal Gaussian elimination process for choosing a suitable representative patch was inspired by the Schubert cell decomposition of the Grassmann manifold; see for example Billey [10], Griffiths and Harris [40], Kleiman and Laksov [58], Kresch [60], Postnikov [83], Sottile [92] and, in a somewhat different vein, Kodama [59]. Since the Grassmann manifold is the disjoint union of Schubert cells, the question is, can we express the flow on the Grassmann manifold as a flow on a linear combination of Schubert cycles, thereby avoiding the need to change coordinate patches (see Griffiths and Harris and also Ravi, Rosenthal and Wang [86])? In other words can we construct the corresponding flow on the cohomological ring of Schubert varieties (Chern [22]; Fulton [35])?

Acknowledgements

We would especially like to thank the anonymous referee #2, who coined the following phrase for the Riccati flow in an earlier version of this manuscript: *this approach is more of Gaussian elimination type (including the question of pivoting, which is not discussed here).* This comment eventually lead us to the Grassmann Gaussian elimination method we investigate in this paper. We would also like to thank referee #1 for useful background on the history of the Evans function, and referee #3 for making us aware of the control theory literature associated with this topic. Chris Jones, Yuri Latushkin, Bob Pego, Bjorn Sandstede and Arnd Scheel organised a workshop at AIM in Palo Alto in May 2005 on *Stability Criteria for Multi-Dimensional Waves and Patterns*, which instigated the topic of this paper. All three authors were visiting the Isaac Newton Institute in the Spring of 2007 when this research was initiated. We would like to thank Arieh Iserles and Ernst Hairer for inviting us and providing so much support and enthusiasm. We are also indebted to the facilities at the Isaac Newton Institute which were invaluable. We also thank Jitse Niesen, Jacques Vanneste and Antonella Zanna for stimulating discussions on this work. Veerle Ledoux is a postdoctoral fellow of the Fund of Scientific Research—Flanders (F.W.O.—Vlaanderen). Vera Thümmler was supported by CRC 701: Spectral Structures and Topological Methods in Mathematics.

References

[1] H. Abou–Kandil, G. Freiling, V. Ionescu and G. Jank, *Matrix Riccati equations in control and systems theory*, Systems and control: Foundations and applications, Birkhäuser, 2003.

[2] J.C., Alexander, R. Gardner, and C.K.R.T. Jones, *A topological invariant arising in the stability analysis of traveling waves*, J. Reine Angew. Math. 410 (1990), pp. 167–212.

[3] J.C. Alexander and R. Sachs, *Linear stability of solitary waves of a Boussinesq-type equation: a computer assisted computation*, preprint 30 Apr, 1999.

[4] L. Allen, *Modelling dolphin hydrodynamics: The numerical analysis and hydrodynamic stability of flow past compliant surfaces*, PhD Thesis, University of Surrey, 2001.

[5] L. Allen and T.J. Bridges, *Numerical exterior algebra and the compound matrix method*, Numer. Math. 92(2) (2002), pp. 131–149.

[6] L. Allen and T.J. Bridges, *Hydrodynamic stability of the Ekman boundary layer including interaction with a compliant surface: a numerical framework*, Eur. J. Mech. B Fluids, 22(3) (2003), pp. 239–358.

[7] N.D. Aparicio, S.J.A. Malham and M. Oliver, *Numerical evaluation of the Evans function by Magnus integration*, BIT 45 (2005), pp. 219–258.

[8] N.J. Balmforth, R.V. Craster and S.J.A. Malham, *Unsteady fronts in an autocatalytic system*, Proc. R. Soc. Lond A. 455 (1999), pp. 1401–1433.

[9] J. Billingham and D. Needham, *The development of travelling waves in quadratic and cubic autocatalysis with unequal diffusion rates, I and II*, Phil. Trans. R. Soc. Lond. A, 334 (1991), pp. 1–124, and 336 (1991), pp. 497–539.

[10] S. Billey, *Grassmannians and other Schubert varieties*, talk, April 14, 2007.

[11] D.S. Bindel, J. Demmel and M. Friedman, *Continuation of invariant subspaces for large bifurcation problems*, Technical Report No. UCB/EECS-2006-13, 2006.

[12] S. Bittanti, A.J. Laub and J.C. Willems (Eds.), *The Riccati equation*, Springer–Verlag, 1991.

[13] Å. Björck and G.H. Golub, *Numerical methods for computing angles between linear subspaces*, Math. Comp. 27(123) (1973), pp. 579–594.

[14] T.J. Bridges, G. Derks and G. Gottwald, *Stability and instability of solitary waves of the fifth-order KdV equation: a numerical framework*, Physica D 172(1–4) (2002), pp. 190–216.

[15] T.J. Bridges and S. Reich, *Computing Lyapunov exponents on a Stiefel manifold*, Physica D 156 (3–4) (2001), pp. 213–238.

[16] L.Q. Brin, *Numerical testing of the stability of viscous shock waves*, PhD Thesis, Indiana University, Bloomington, 1998.

[17] L.Q. Brin, *Numerical testing of the stability of viscous schock waves*, Math. of Comput. 70(235) (2000), pp. 1071–1088.

[18] R.W. Brockett and C.I. Byrnes, *Multivariable Nyquist criteria, root loci, and pole placement: a geometric viewpoint*, IEEE Trans. Automat. control 26(1) (1981), pp. 271–284.

[19] E. Celledoni and A. Iserles, *Approximating the exponential from a Lie algebra to a Lie group*, Math. Comp. 69 (2000), pp. 1457–1480.

[20] E. Celledoni and B. Owren, *On the implementation of Lie group methods on the Stiefel manifold*, Numer. Algorithms 32 (2003), pp. 163–183.

[21] H.-C. Chang, E.A. Demekhin and D.I. Kopelevich, *Local stability theory of solitary pulses in an active medium*, Physica D 97 (1996), pp. 353–375.

[22] S.S. Chern, *Complex manifolds without potential theory*, Van Nostrand Mathematical Studies #15, 1967.

[23] C.–C. Chou and R.E. Wyatt, *Computational method for the quantum Hamilton–Jacobi equation: Bound states in one dimension*, J. Chem. Phys. 125(174103) (2006), pp. 1–10.

[24] C.–C. Chou and R.E. Wyatt, *Riccati differential equation for qunatum mechanical bound states: comparison of numerical integrators*, Int. J. Quant. Chem. 108 (2008), pp.238–248.

[25] S. Coombes and M. R. Owen, *Evans function for integral neural field equations with heaviside firing rate function*, submitted to SIAM J. Appl. Dyn. Syst. (2004).'

[26] I. Coskun, *Grassmannians: the first example of a moduli space*, MITOpenCourseWare available at `http://ocw.mit.edu/NR/rdonlyres/Mathematics/18-727Spring-2006`.

[27] J. Deng and S. Nii, *Infinite-dimensional Evans function theory for elliptic eigenvalue problems in a channel*, J. Differential Equations 225 (2006), pp. 57–89.

[28] G. Derks, U. Ebert and B. Meulenbroek, *Laplacian instability of planar streamer ionization fronts - an example of pulled front analysis*, Journal Nonl. Science, 2008.

[29] A. Dhooge, W. Govaerts and Y.A. Kuznetsov, *MATCONT: a MATLAB package for numerical bifurcation analysis of ODEs*, ACM Trans. Math. Software, 29(2) (2003), pp. 141–164.
[30] L. Dieci and E.S. Van Vleck, *Orthonormal integrators based on Householder and Givens transformations*, Future Generation Computer Systems 19(3) (2003) Special issue: Geometric numerical algorithms, pp. 363–373.
[31] A. Doelman, R.A. Gardner and T.J. Kaper, *Stability analysis of singular patterns in the 1D Gray-Scott model: A matched asymptotics approach*, Physica D 122 (1998), pp. 1–36.
[32] L.O. Drury, *Numerical solution of Orr-Sommerfeld-type equations*, J. Comput. Phys. 37(1) (1980), pp. 133–139.
[33] A. Edelman, T.A. Arias and S.T. Smith, *The geometry of algorithms with orthogonality constraints*, SIAM. J. Matrix Anal. Appl. 20(2) (1998), pp. 303–353.
[34] J.W. Evans, *Nerve axon equations, IV: The stable and unstable impulse*, Indiana Univ. Math. J. 24 (1975), pp. 1169–1190.
[35] W. Fulton, *Young tableaux*, London Mathematical Society Student Texts 35, Cambridge University Press, 1997.
[36] F. Gesztesy, Y. Latushkin and K.A. Makarov, *Evans functions, Jost functions, and Fredholm determinants*, Arch. Rational Mech. Anal. 186 (2007), pp. 361–421.
[37] F. Gesztesy, Y. Latushkin and K. Zumbrun, *Derivatives of (modified) Fredholm determinants and stability of standing and travelling waves*, arXiv:0802.1665v1, 12 Feb 2008.
[38] S.K. Gray and D.E. Manopoulous, *Symplectic integrators tailored to the time-dependent Schrödinger equation*, J. Chem. Phys. 104(18) (1996), pp. 7099–7112.
[39] J. Greenberg and M. Marletta, *Numerical solution of non-self-adjoint Sturm-Liouville problems and related systems*, SIAM J. Numer. Anal. 38(6) (2000), pp. 1800–1845.
[40] P. Griffiths and J. Harris, *Principles of algebraic geometry*, Wiley Classics Library Edition, 1994.
[41] V. Gubernov, G.N. Mercer, H.S. Sidhu and R.O. Weber, *Evans function stability of non-adiabatic combustion waves*, Proc. R. Soc. Lond. A 460 (2004), pp. 2415–2435.
[42] E. Hairer, C. Lubich and G. Wanner, *Geometric Numerical Integration*, Springer Series in Computational Mathematics, 2002.
[43] D. Henry, *Geometric theory of semilinear parabolic equations*, Lecture Notes in Mathematics 840, Springer–Verlag, 1981.
[44] R. Hermann and C. Martin, *Applications of Algebraic geometry to systems theory – part I*, IEEE Trans. Automat. Control 22(1) (1977), pp. 19–25.
[45] R. Hermann and C. Martin, *Lie theoretic aspects of the Riccati equation*, NASA Report WP2-3:30.
[46] R. Hermann and C. Martin, *Periodic solutions of the Riccati equation*, NASA Report TP3-3:00, IEEE (1980).
[47] R. Hermann and C. Martin, *Lie and Morse theory for periodic orbits of vector fields and matrix Riccati equations, I: General Lie-theoretic methods*, Mathematical Systems Theory 15 (1982), pp. 277–284.
[48] R. Hermann and C. Martin, *Lie and Morse theory for periodic orbits of vector fields and matrix Riccati equations, II*, Mathematical Systems Theory 16 (1983), pp. 297–306.
[49] J. Humpherys and K. Zumbrun, *An efficient shooting algorithm for Evans function calculations in large systems*, Physica D 220 (2006), pp. 116–126.
[50] J. Humpherys, B. Sandstede and K. Zumbrun, *Efficient Computation of Analytic Bases in Evans Function Analysis of Large Systems*, Numer. Math. 103(4) (2006), pp. 631-642.
[51] J.M. Hutson, *Coupled channel methods for solving the bound-state Schrödinger equation*, Computer Physics Communications 84 (1994), pp. 1–18.
[52] A. Iserles, A. Marthinsen and S.P. Nørsett, *On the impementation of the method of Magnus series for linear differential equations*, University of Cambridge Numerical Analysis Reports, DAMTP 1998/NA2, 1998.
[53] A. Iserles and A. Zanna, *Efficient computation of the matrix exponential by generalized polar decompositions*, SIAM J. Numer. Anal. 42(5) (2005), pp. 2218–2256.
[54] A. Iserles, H. Z. Munthe-Kaas, S. P. Nørsett, and A. Zanna, *Lie-group methods*, Acta Numer. (2000), pp. 215–365.
[55] L.Gr. Ixaru, *Special techniques related to the CP methods for the coupled channel Schrödinger equation*, talk given at Workshop Numerical Approach of Oscillatory functions 2008, Ghent.

[56] B.R. Johnson, *New numerical methods applied to solving the one-dimensional eigenvalue problem*, J. Chem. Phys. 67(9) (1977), pp. 4086–4093.
[57] T. Kapitula and B. Sandstede, *A novel instability mechanism for bright solitary-wave solutions to the cubic-quintic Ginzburg–Landau equation*, J. Opt. Soc. Amer. B 15 (1998), pp. 2757–2762.
[58] S.L. Kleiman and AD. Laksov, *Schubert calculus*, Amer. Math. Month. 79(10) (1972), pp. 1061–1082.
[59] Y. Kodama, *Young diagrams and N-soliton solutions of the KP equation*, J. Phys. A: Math. Gen. 37 (2004), pp. 11169–11190.
[60] A. Kresch, *Flag varieties and Schubert calculus*, preprint, July 2005.
[61] S. Krogstad, *A low complexity Lie group method on the Stiefel manifold*, Reports in Informatics, ISSN 0333-3590, 2001.
[62] S. Lafortune and J. Lega, *Instability of local deformations of an elastic rod*, Physica D 182 (2003), pp. 103–124.
[63] S. Lafortune and P. Winternitz, *Superposition formulas for pseudounitary Riccati equations*, J. Math. Phys. 37 (1996). pp. 1539-1550.
[64] V. Ledoux, *Study of special algorithms for solving Sturm-Liouville and Schrödinger equations*. PhD Thesis, Universiteit Gent, 2007.
[65] V. Ledoux, M. Vand Daele and G. Vanden Berghe, *A numerical procedure to solve the multichannel Schrödinger eigenvalue problem*, Comp. Phys. Commun. 176 (2007). pp. 191-199.
[66] V. Ledoux, S.J.A. Malham, J. Niesen and V. Thümmler, *Computing stability of multidimensional travelling waves*, submitted to SIADS, 2008.
[67] J.C. Light and R.B. Walker, *An R matrix approach to the solution of coupled equations for atom-molecule reactive scattering*, J. Chem. Phys. 65(10) (1976), p. 4272–4282.
[68] W. Magnus, *On the exponential solution of differential equations for a linear operator*, Comm. Pure Appl. Math., 7 (1954), pp. 649–673.
[69] D.E. Manopoulous and S.K. Gray, *Symplectic integrators for the multichannel Schrödinger equation*, J. Chem. Phys. 102(23) (1995), pp. 9214–9227.
[70] J. E. Marsden and T. S. Ratiu, *Introduction to mechanics and symmetry*, Second edition, Springer, 1999.
[71] C. Martin and R. Hermann, *Applications of algebraic geometry to systems theory: The McMillan degree and Kronecker indicies of transfer functions as topological and holomorphic system invariants*, SIAM J. Control Optim. 16(5) (1978), pp. 743–755.
[72] M.J. Metcalf, J.H. Merkin and S.K. Scott, *Oscillating wave fronts in isothermal chemical systems with arbitrary powers of autocatalysis*, Proc. R. Soc. Lond. A 447 (1994), pp. 155-174.
[73] C. Meyer, *Matrix analysis and applied linear algebra*, SIAM, 2000.
[74] J.W. Milnor and J.D. Stasheff, *Characteristic classes*, Annals of mathematics studies 76, Princeton University Press, 1974.
[75] C. Moler and C. Van Loan, *Nineteen dubious ways to compute the exponential of a matrix, twenty-five years later*, SIAM Rev. 45 (2003), pp. 3–49.
[76] R. Montgomery, *A tour of subRiemannian geometries, their geodesics and applications*, Mathematical Surveys and Monographs 91, American Mathematical Society, 2002.
[77] H. Munthe-Kaas, *High order Runge–Kutta methods on manifolds*, Appl. Numer. Math., 29 (1999), pp. 115–127.
[78] H. Munthe-Kaas and A. Zanna, *Generalized polar decompositions for the approximation of the matrix exponential*, SIAM J. Matrix Anal. Applic. 23(3) (2002), pp. 840–862.
[79] S. Nii, *An extension of the stability index for traveling-wave solutions and its application to bifurcations*, SIAM J. Math. Anal. 28(2) (1997), pp. 402–433.
[80] E. Oja, *A Simplified Neuron Model as a Principal Component Analyzer*, J. Math. Biology 15 (1982), pp. 267–273.
[81] P.J. Olver, *Equivalence, Invariants, and symmetry*, Cambridge University Press, 1995.
[82] R.L. Pego and M.I. Weinstein, *Eigenvalues and instabilities of solitary waves*, Phil. Trans. R. Soc. Lond. A 340 (1992), pp. 47–94.
[83] A. Postnikov, *Total positivity, Grassmannians, and Networks*, arXiv:math/060976v1 27 Sep 2006.
[84] H. Prüfer, *Neue Herleitung der Sturm–Liouvilleschen Reihenentwicklung*, Math. Ann. 95 (1923), pp. 499–518.

[85] J.D. Pryce, *Numerical solution of Sturm–Liouville problems*, Monographs of Numerical Analysis, Oxford Science Publications, Clarendon Press, 1993.
[86] M.S. Ravi, J. Rosenthal and X. Wang, *Dynamic pole assignment and Schubert calculus*, SIAM J. Control Optim. 34(3) (1996), pp. 813–832.
[87] J. Rosenthal, *The Hermann–Martin curve*, preprint report.
[88] B. Sandstede, *Stability of travelling waves*, In Handbook of Dynamical Systems II, B. Fiedler, ed., Elsevier (2002), pp. 983–1055.
[89] B. Sandstede and A. Scheel, *Curvature effects on spiral spectra: Generation of point eigenvalues near branch points*, Phys. Rev. E 73 106217, 2006.
[90] J. Schiff and S. Shnider, *A natural approach to the numerical integration of Riccati differential equations*, SIAM J. Numer. Anal. 36(5) (1999), pp. 1392–1413.
[91] M.A. Shayman, *Phase portrait of the matrix Riccati equation*, SIAM J. Control Optim. 24(1) (1986), pp. 1–65.
[92] F. Sottile, *Rational curves on Grassmannians: systems theory, reality, and transversality*, arXiv:math/0012079v1 11 Dec 2000.
[93] N. Steenrod, *The topology of fibre bundles*, Princeton University Press, 1951.
[94] J. Swinton and J. Elgin, *Stability of travelling pulse solutions to a laser equation*, Phys. Lett. A 145(8–9) (1990), pp.428–433.
[95] D. Terman, *Stability of planar wave solutions to a combustion model*, SIAM J. Math. Anal., 21 (1990), pp. 1139–1171.
[96] F.W. Warner, *Foundations of differentiable manifolds and Lie groups*, Graduate texts in mathematics, Springer, 1983.
[97] W-Y. Yan, U. Helmke and J.B. Moore, *Global analysis of Oja's flow for neural networks*, IEEE Transactions on Neural Networks 5(5) (1994), pp. 674–683.
[98] X. Ying and I. Katz, *A reliable argument principle algorithm to find the number of zeros of an analytic function in a bounded domain*, Numer. Math. 53 (1988), pp. 143–163.
[99] M.I. Zelikin, *Control theory and optimization I: Homogeneous spaces and the Riccati equation in the calculus of variations*, Encyclopaedia of Mathematical Sciences, Volume 86, Springer–Verlag 2000.

[1]Vakgroep Toegepaste Wiskunde en Informatica, Ghent University, Krijgslaan, 281-S9, B-9000 Gent, Belgium, [2]Department of Mathematics, Heriot-Watt University, Edinburgh EH14 4AS, UK, [3]Fakultät für Mathematik, Universität Bielefeld, 33501 Bielefeld, Germany